Science of the Total Environment 829 (2022) 154681

Contents lists available at ScienceDirect

Science of the Total Environment

journal homepage: www.elsevier.com/locate/scitotenv

Combining NDVI, PRI and the quantum yield of solar-induced fluorescence improves estimations of carbon fluxes in deciduous and evergreen forests

Daniel Kováč [a,*], Alexander Ač [a], Ladislav Šigut [a], Josep Peñuelas [a,b,c], John Grace [a,d], Otmar Urban [a]

[a] Global Change Research Institute of the Czech Academy of Sciences, Bělidla 986/4a, 603 00 Brno, Czech Republic
[b] CSIC, Global Ecology Unit CREAF-CSIC-UAB, E-08193 Bellaterra, Catalonia, Spain
[c] CREAF, E-08193 Cerdanyola del Vallès, Catalonia, Spain
[d] School of GeoSciences, University of Edinburgh, Crew Bldg, Kings Bldgs, Alexander Crum Brown Rd, Edinburgh EH9 3FF, UK

HIGHLIGHTS

- The seasonal dynamics of optical indices over beech and spruce forests are evaluated.
- Fluorescence and PRI are estimated from one spectral signature.
- NDVI and PRI show different seasonal dynamics in deciduous and evergreen forests.
- Solar-induced fluorescence at 760 nm shows seasonal dynamics with APAR and GPP.
- Combining all parameters improves GPP estimation across the entire season.

GRAPHICAL ABSTRACT

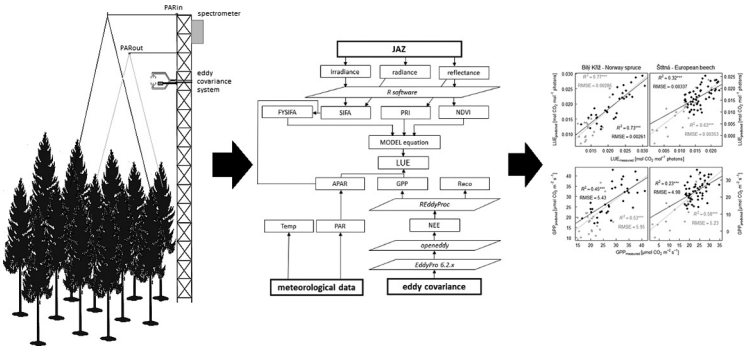

ARTICLE INFO

Article history:
Received 3 January 2022
Received in revised form 28 February 2022
Accepted 15 March 2022
Available online 18 March 2022

Editor: Pavlos Kassomenos

Keywords:
3-FLD
Chlorophyll fluorescence
Eddy covariance fluxes
NDVI
Photochemical reflectance index
Seasonal dynamics

ABSTRACT

We used automated spectroradiometers to continuously monitor changes in the optical parameters of phenological and photosynthetic traits in beech and spruce forests. We examined seasonal variations in the normalized difference vegetation index (NDVI), photochemical reflectance index (PRI), and solar-induced fluorescence in the oxygen A band (SIFA) that was estimated using a 3-FLD discrimination method from radiance data. The optical parameters tracked the activation and cessation of photosynthesis in spring and autumn. Data at photon fluxes >1200 μmol m^{-2} s^{-1} during extended noon hours were used to link the seasonal PRI and SIFA variations to the dynamics of photosynthesis. Seasonal PRI was significantly correlated with photosynthetic light-use efficiency (LUE) with R^2 values of 0.66 and 0.48 for the measurements in beech and spruce forests, respectively. SIFA emissions were significantly correlated with the gross primary production (GPP) of the evergreen spruce forest (R^2 = 0.47), but R^2 was only 0.13 when measured in the beech forest. The correlations between the optical parameters and GPP or LUE, however, tended to be lower when using a dataset with constant NDVI. Introducing an equation combining NDVI, PRI, and the quantum yield of SIFA emission increased R^2 for LUE estimation to 0.77 in the spruce forest and 0.63 in the beech forest. GPP was estimated from the parametric equation with improved accuracy reaching R^2 = 0.53 and RMSE = 5.95 μmol CO_2 m^{-2} s^{-1} in spruce forest and R^2 = 0.58 and RMSE = 5.23 μmol CO_2 m^{-2} s^{-1} in beech forest. Parametric equations were more efficient in estimating photosynthesis in datasets that consisted of an entire season's data. By combining NDVI, PRI and the quantum yield of SIFA, we could thus substantially improve estimations of carbon fluxes in diverse deciduous and evergreen canopies.

* Corresponding author.
E-mail address: kovac.d@czechglobe.cz (D. Kováč).

http://dx.doi.org/10.1016/j.scitotenv.2022.154681

1. Introduction

It is clear that forests are strong carbon sinks, both during early stages of growth and when in their mature phase (Pan et al., 2011). The natural processes of photosynthesis and respiration represent major carbon fluxes, far exceeding the emissions from fossil fuel burning. However, it is also clear that forests are vulnerable to climatic stress, particularly drought and other extreme events. An important goal in forest research is therefore to be able to detect climatic influences on photosynthesis using remote sensing (Nichol et al., 2000). The establishment of networks of CO_2 flux towers was an important step forward (Baldocchi, 2020). They provide points of reference for the remote sensing of photosynthesis, and now there are several hundred of them in the world. When plants are stressed, perturbations of the photosystems may be detectable remotely, from a tower, an aircraft or satellite. The present work is a contribution to the remote detection of the rates of photosynthesis.

Remote sensing of photosynthesis is based on the fundamental photochemical processes that underly the capture of solar energy. In photosynthesis, a balance must be struck between maximizing the capture of solar energy and minimizing the photochemical damage to the photochemical apparatus itself. Photoprotective mechanisms have therefore evolved to allow the release of excessive solar energy by two main processes: nonphotochemical quenching (NPQ) and fluorescence. The fraction of absorbed energy that can be used in photosynthesis depends on many factors, but is diminished by physiological stress (Zarco-Tejada et al., 2000). Remote detection of the rate of canopy photosynthesis is an important goal, which might be achieved if NPQ and fluorescence can be measured with the required degree of precision.

NPQ is mediated by the pigments of the xanthophyll cycle, the dynamics of which are detectable by the reflectance changes at 531 nm, measurable as the photochemical reflectance index (PRI) (Peñuelas et al., 1995). PRI associates optical data with the photosynthetic light-use efficiency (LUE) of the vegetation. The suitability of PRI for detecting photosynthesis has been widely examined and general accepted (Garbulsky et al., 2011; Peñuelas et al., 2011). Significant limitations of the applicability of PRI for estimating instantaneous photosynthesis rates, however, have been reported. They are most likely due to the variations associated with the ratios of chlorophylls to carotenoids (Zhang et al., 2016). Other variations in the canopy level PRI are further associated with the sun elevation, which alters exposure of the foliar area from which the signal comes (Barton and North, 2001) and changes the apparent foliar area that contributes to CO_2 uptake.

Fluorescence is the radiative emission that comes from chlorophyll molecules themselves. Usefulness of fluorescent emissions for detecting canopy stress or photosynthesis has often been demonstrated. Advances in measuring techniques for estimating fluorescence from passive instruments have provided opportunities to use passive fluorescent signals as a measure of plant stress and hence, photosynthesis (Damm et al., 2010). The quantum yield of fluorescence, which is defined as the ratio of the number of emitted to absorbed photons, depends on the functional status of photochemical quenching and NPQ (Lichtenthaler and Rinderle, 1988). Much attention is given to signals associated with the fluorescence peak at 740 nm. The signal is not affected by overlaps between spectra of fluorescence emission and chlorophyll absorption. An emission peak at 740 nm generally increases with chlorophyll content due to scattering effects in the near-infrared spectrum (van Wittenberghe et al., 2013).

Methods to estimate fluorescence from passive measurements rely on depth discrimination of the oxygen absorption band near 760 nm (O_2A) by applying infilling methods for the spectra to the Fraunhofer line (Julitta et al., 2016; Perez-Priego et al., 2005). The most commonly used methods are based on Fraunhofer Line Depth (FLD) discrimination. The most frequently used FLD methods are labelled as 3-FLD, sFLD or iFLD. The methods differ in principles, complexity and numbers of wavebands used for fluorescence estimation depending on the type of application or parameters of measurements. It has been shown that the relationship between photosynthesis and solar-induced fluorescence in the telluric oxygen absorption band O_2A (SIFA) probably relies on the dependence of fluorescent emission on the amount of absorbed photosynthetically active radiation (APAR) (Goulas et al., 2017). The sensitivity of fluorescence to other factors, such as vegetation phenology, has also been reported (Daumard et al., 2012). Similar to PRI, SIF of the vegetated areas depends on many additional factors, such as the geometric arrangement of the measurement, measurement conditions or canopy structure (Zhang et al., 2020).

The first attempts to measure the dynamics of photosynthesis using spectroradiometers in the field are associated with measurements of NDVI, which estimate the changes in total green biomass over short periods of time (Gamon et al., 1995). NDVI is typically used to evaluate seasonal phenology or vegetation productivity because it gradually increases with growth and decreases with senescence. NDVI was not found so useful for measuring changes in evergreen species, which exhibit only limited variations in vegetation greenness. Likewise, this limitation applies to deciduous vegetation over the summer period. Fluorescence and PRI data inputs to the models may add accuracy to photosynthesis estimations as these parameters show pronounced changes within days and across the season with diverse environmental conditions. PRI and fluorescent emission represent optically measured photoprotective mechanisms that work in parallel (Chen et al., 2019; van der Tol et al., 2014); both are dynamic with light and both can be detected using field spectral systems. Therefore, we aim to study whether combining all of these approaches (i.e., SIFA, PRI, and NDVI) can improve estimations of carbon fluxes in diverse deciduous and evergreen canopies.

The data collected using the tower spectral systems may thus be used for intensive and extensive modeling of canopy GPP and LUE seasonality. Advances in measuring techniques allow for measurements that provide integrated data and may explain seasonal variations of fluorescence together with other canopy parameters. The results from the measurements may further reveal the potentials and limitations of spectral measurements for monitoring ecosystem functioning. Tower-based reflectance and SIFA retrieval algorithms allow the calculation of parameters for measurements under a variety of environmental conditions and provide better indications of signal variability with systems change (Cogliati et al., 2015; Paul-Limoges et al., 2018). We used data from automated spectroradiometers that were placed above evergreen spruce and deciduous beech forests to study the dynamic changes in NDVI, PRI, and SIFA along with the changes in seasonal phenology and GPP. We aimed to explore how the changes in optical parameters are correlated with changes in photosynthetic CO_2 uptake and to evaluate whether the combination of optical parameters can improve the estimations of canopy carbon fluxes.

2. Materials and methods

2.1. Site descriptions

This study used measurements at mountainous ecosystem stations, Bílý Kříž and Štítná, in the Czech Republic that are a part of the CzeCOS (http://www.czecos.cz/, Fig. 1) and ICOS (http://icos-cp.eu) infrastructures. The Bílý Kříž site is located in the northeastern Czech Republic (49°30′07.474″N, 18°32′12.777″E) at 875 m a.s.l. The forest is on a 13° slope oriented south-southwest, approximately 100 m downslope of a mountain crest that is oriented west to east (McGloin et al., 2018). The ecosystem consists of a coniferous evergreen Norway spruce (*Picea abies* L. Karst.) forest. The stand was 37 years old and 17 m high in the year of measurement (2018) with an estimated leaf area index (one-sided projected) of 8.2 m^2 m^{-2} in that year. The mean annual temperature at the site is 6.8 °C, and the mean annual precipitation is 1114 mm. The Štítná site is located in the southeastern Czech Republic (49°02′09.510″N, 17°58′11.640″E) at 540 m a.s.l. The site is spread on a slope that is oriented west-southwest. The Štítná site is dominated by European beech (*Fagus sylvatica* L.) trees

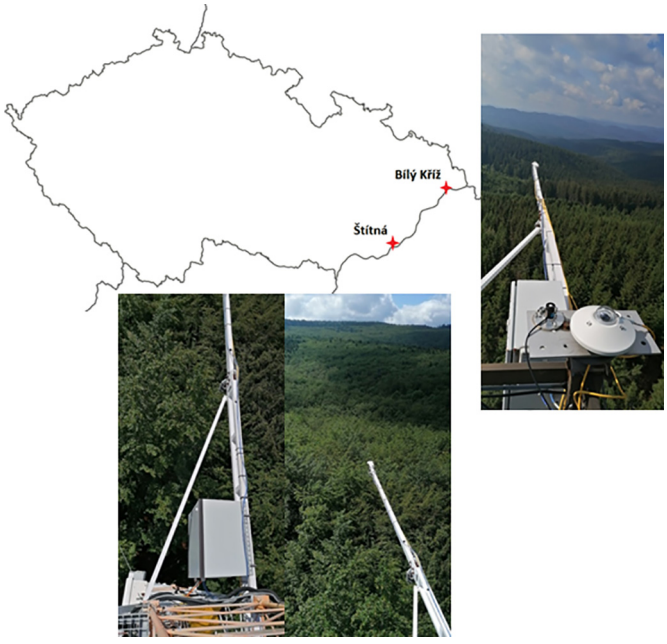

Fig. 1. Housing boxes for the spectrometers mounted on top of the eddy-covariance towers and shoulders conducting measuring fiber optic components at the sides of the towers. Measurements were conducted at the Bílý Kříž ecological station (ES) in the Norway spruce stand and the Štítná ecological station in the European beech stand.

which were 116 years old and averaged 31 m in height at the time of measurements in 2017. The leaf area index at the canopy crown (one-sided) was 5.3 m^2m^{-2} during the summer. The mean annual temperature and precipitation were 9.1 °C and 678 mm, respectively. Measurements and data processing in presented work used instrumentation shown in workflow diagram (Fig. 2).

2.2. Estimation of carbon fluxes at experimental sites

Eddy covariance (EC) was used to measure CO_2 turbulent fluxes at the Bílý Kříž and Štítná forest sites. Both EC systems consisted of HS-50 ultrasonic anemometers (Gill Instruments, Lymington, UK) and LI-7200 infrared gas analyzers (LI-COR Biosciences, Lincoln, NE, USA). The instruments were installed on a meteorological tower at heights of 25 m (Bílý Kříž) and 44 m (Štítná) above ground level and followed the standardized protocols for ICOS measurements. The processing of raw EC data obtained at 20 Hz included spike detection and removal, time-lag compensation, sonic-temperature correction, and high- and low-frequency spectral corrections. Coordinate rotation was performed using the planar-fit method. Fluxes were calculated at half-hourly intervals using block averaging. All EC processing and calculations were performed using EddyPro version 6.2.x (LI-COR Biosciences, USA).

The quality of the EC measurements was thoroughly checked using the *openeddy* R package (R Core Team, 2020; https://github.com/lsigut/openeddy; see McGloin et al., 2018 for details). Measured CO_2 fluxes were filtered based on the friction velocity threshold calculated by using the moving-point method (Papale et al., 2006), and gaps were filled using marginal distribution sampling (Reichstein et al., 2005). Half-hourly CO_2 fluxes were assumed to represent net ecosystem exchange (NEE; μmol CO_2 m^{-2} s^{-1}). NEE was partitioned into GPP and ecosystem respiration, as described by Lasslop et al. (2010) using the *REddyProc* R package (Wutzler et al., 2018).

Air temperature and humidity were measured using a shielded HMP45C probe (Vaisala, Helsinki, Finland) placed on the tower above the forest. Incoming and reflected photosynthetically active radiation (PAR) at the forest sites within the spectral range of 400–700 nm were measured using an LI-190/R quantum sensor (LI-COR Biosciences, USA). Absorbed PAR (APAR) for the forest canopies was calculated as the difference between incoming PAR and PAR reflected from the forests. Transmitted PAR to the forest floor was not considered in APAR calculation since it depends on sensors layout and produces uncertainties in the results. LUE was calculated as the ratio between half-hourly averages of GPP and APAR as:

$$\mathrm{LUE} = \frac{\mathrm{GPP}}{\mathrm{APAR}}. \quad (1)$$

2.3. Spectral measurements at the ecosystem stations

Spectral measurements for estimating NDVI, PRI, and fluorescence in the forests used custom-made spectrometers consisting of two JAZ spectrometers (Ocean Optics, Dunedin, FL, USA). The instrument was introduced by Kováč et al. (2018). The method uses hemispherical upward- and downward-directed (field-stop) sensors that measure incoming and upwelling radiance (Fig. 3). Each JAZ sensor collects data in the spectral range between 340 and 1025 nm in 2048 channels with a spectral resolution of 1 nm. Data were acquired at steps of approximately 0.3 nm. The two spectrometers enabled simultaneous determinations of incoming and reflected radiation at both sites with an automated routine adjusting the integration time to the intensity of incoming radiation to optimize the signal-to-noise ratio (Pacheco-Labrador and Martin, 2014). The systems were calibrated before the start of measurements in the early spring. The measuring system was calibrated using a Spectralon panel that reflected downwelling irradiance under clear skies. Reflectance was calculated from digital count units. The JAZ spectrometers were calibrated for the acquisition of radiometric units on-site using an HL-2000 calibration lamp (Ocean Optics, USA). Boxcar in the calibration procedure was set to 0. Similarly, spectra were measured without smoothing with the boxcar set to 0. Upwelling radiance and downwelling irradiance were measured every 5 min. The optical parameters were calculated as half-hourly averages to match the EC outputs. The spectrometers were housed in cooled insulated metallic boxes to ensure stable measurements at temperatures

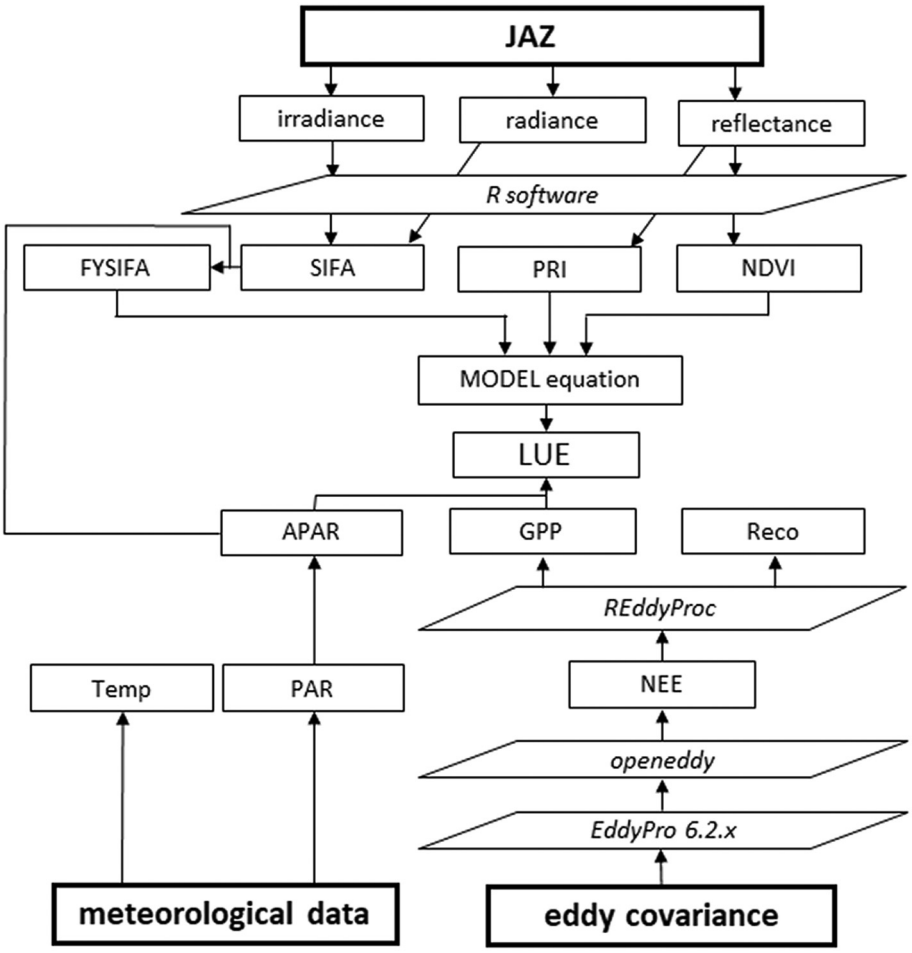

Fig. 2. Workflow of the data measurements and data processing in the experiment.

optimally ranging between 20 and 30 °C. Measurements started at 06:00 and ended at 18:00 every day. All calibrations and measurements were identical for both sites.

The fiber optic components of the spectrometers were mounted on the tops of the meteorological towers at a distance of approximately 4 m to the south of the tower to avoid artificial shading of the measured area (Fig. 1). Spectral data at Bílý Kříž (spruce forest) were measured at a height of 20 m above the canopy. Sampling area corresponded to approximately 80 m^2 and covered crowns of seven spruce trees in total. Examples of irradiance spectra of incoming light, spectra of reflected radiance of the forest and adjacent reflectance signature are shown in Fig. 3. The footprint of the measurements at Štítná (beech forest) was approximately 25 m^2 and covered only the crown of one tree. A LiDAR scan of the area was processed at both sites to identify changes in shadows within the field of view of 15% during the season. The estimated changes in canopy shadows were calculated for sun elevations 25–65° and sun azimuth angles 50–250°.

NDVI was calculated in two variants involving red or red-edge reflectance wavebands as described by Datt (1999):

$$NDVI1 = \frac{R_{780} - R_{680}}{R_{780} + R_{680}} \quad (2)$$

and

$$NDVI2 = \frac{R_{780} - R_{720}}{R_{780} + R_{720}}. \quad (3)$$

PRI was calculated following Gamon et al. (1992, 1997):

$$PRI = \frac{R_{531} - R_{570}}{R_{531} + R_{570}}. \quad (4)$$

SIFA was estimated using the FLD infilling discrimination method (Plascyk, 1975). The 3-FLD equation was applied to the telluric oxygen absorption band O_2A (at around 760.4 nm), to estimate fluorescence based on the direct comparison between solar irradiance and radiance emitted by the vegetation (Meroni et al., 2009). Zoomed in spectra in the region that is used to estimate SIFA from measured data are shown in Fig. 4. Estimation was based on measuring the response in a single band with the maximum absorption by oxygen (Fig. 4). SIFA was calculated as:

$$SIFA = \frac{L(\lambda_{in}) - \frac{E(\lambda_{in})\cdot\left(w_{left}\cdot L(\lambda_{left}) + w_{right}\cdot L\left(\lambda_{right}\right)\right)}{w_{left}\cdot E(\lambda_{left}) + w_{right}\cdot E\left(\lambda_{right}\right)}}{1 - \frac{E(\lambda_{in})}{w_{left}\cdot E(\lambda_{left}) + w_{right}\cdot E\left(\lambda_{right}\right)}}, \quad (5)$$

where

$$w_{left} = \frac{\lambda_{in} - \lambda_{left}}{\lambda_{right} - \lambda_{left}} \quad (6)$$

and

$$w_{right} = \frac{\lambda_{right} - \lambda_{in}}{\lambda_{right} - \lambda_{left}}. \quad (7)$$

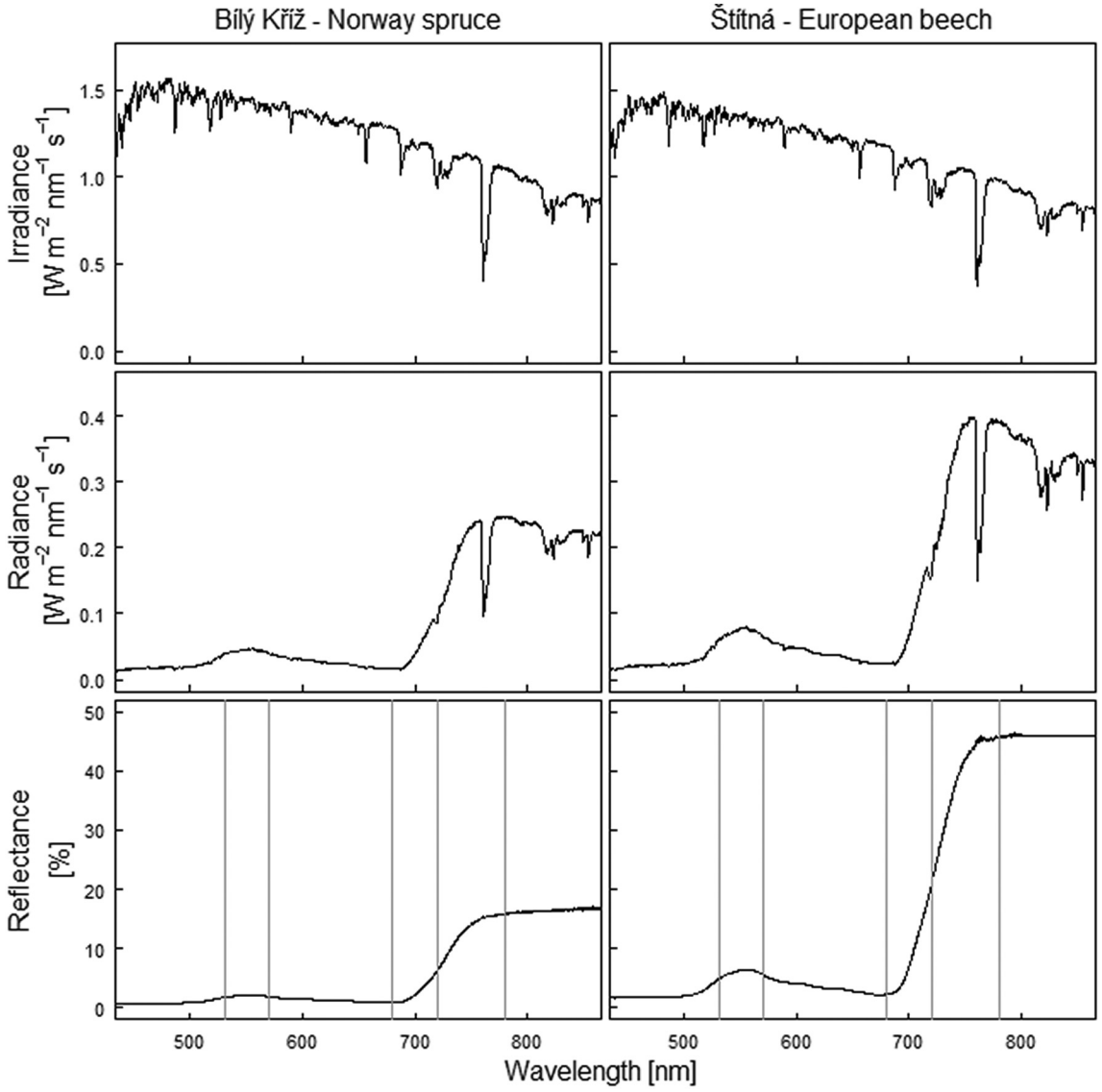

Fig. 3. Spectra of irradiance and reflected radiance at the Bílý Kříž and Štítná ecological stations measured at midday on a sunny day in July. Associated reflectance curves are shown in the bottom panels. Gray vertical lines indicate the wavelengths used for estimating NDVI and PRI from the reflectance.

$L(\lambda_{left})$ and $L(\lambda_{right})$ represent the radiances in the left and right shoulders of the Fraunhofer band, respectively, and $E(\lambda_{left})$ and $E(\lambda_{right})$ similarly represent the solar irradiances in corresponding wavebands. w_{left} and w_{right} are the weights of the two bands outside the Fraunhofer band. All calculations were made in R software (R Core team, 2020). Wavelengths of 756.2 nm (λ_{left}), 760.4 nm (λ_{in}), and 775.3 nm (λ_{right}) were specifically selected to estimate SIF in the O_2A band. Selected wavebands differ between 4 used spectrometers by hundredths of nm. These small shifts in wavebands do not introduce much instability to SIFA estimations.

Spectroradiometers with a spectral resolution of 1 nm have the potential to provide reliable fluorescence data (Julitta et al., 2016). We expect the error lower than 10% in daily measured data after applying the equation to the reflected radiance and irradiance data (Fig. 5), if the data are measured following described calibration of the measuring system. The assumption is made based on observing estimated fluorescence dynamics for the non-fluorescing target, which was the Spectralon panel. The dynamic was measured on a cloudless day under changing sun zenith and azimuth angles in late June. The error can reach ±5% for measurements at Bílý Kříž site around midday, where absolute SIFA reaches 1 mW m^{-2} sr^{-1} nm^{-1}. At Štítná site with higher SIFA at around 3 mW m^{-2} sr^{-1} nm^{-1} the propagated error in SIFA can be as high as ±2%. The error propagation can be dependent also on atmospheric effects and scale of measurements. We are not considering such influence on estimated SIFA of forests, which is estimated for measurements from a greater distance for surface with significant topography.

The quantum yield of SIFA (FYSIFA) was calculated as:

$$\mathrm{FYSIFA} = \frac{\mathrm{SIFA}}{\mathrm{APAR\ (nm)}}. \tag{8}$$

The yield of SIFA is expressed per wavelength unit in the PAR region and describes the fraction of photons that are reemitted relative to the photons absorbed by the vegetation cover (Wieneke et al., 2018). The calculated ratio was multiplied by 100 to express the result as a percentage [%] of APAR and to adjust the FYSIFA value for the next step.

2.4. Parametric model equations

NDVI2, PRI, and FYSIFA were combined into a single equation and compared to GPP and LUE. We used an equation introduced by Schickling et al.

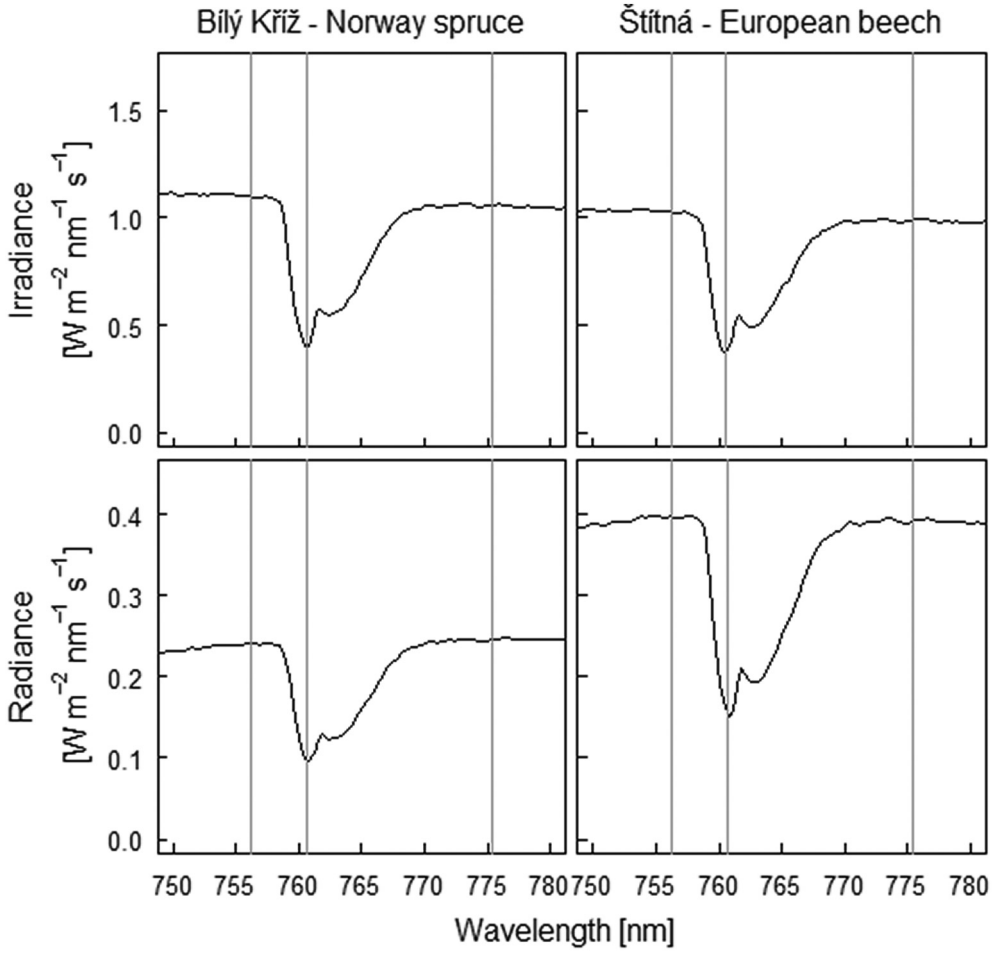

Fig. 4. Zoomed in spectra of irradiance and reflected radiance from the forest in the area surrounding O_2A absorption band at 760.4 nm. Gray vertical lines indicate the wavelengths used for estimating fluorescence emission in the O_2A band from 3-FLD equation.

(2016) as a basis for the modeling. We made a small modification to the equation to parametrize the processes of photosynthesis in the spruce forest. The first constant in the equation was modified to better fit requirements for the modeling using data from spectrometric measurements. The equation to measure LUE and GPP dynamics in the spruce forest looks as follows:

$$\text{Model1} = (0.69 \times PRI \times FYSIFA - 0.09)(0.15 \times NDVI2 + 0.84) \quad (9)$$

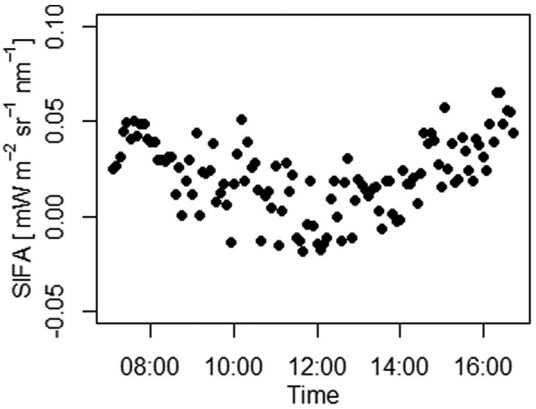

Fig. 5. Daily change in SIFA detected at 5 min frequency for measurements of the Spectralon panel.

The equation was slightly reparametrized to estimate changes in the beech forest based on modeling and fitting of the response in the data:

$$\text{Model2} = (3.88 \times PRI \times FYSIFA - 0.03)(0.23 \times NDVI2 + 0.75). \quad (10)$$

Coefficients in linear equations were optimized to achieve the best fit (1:1) between modeled and measured values of LUE and GPP. The aim of the analyses is to estimate photosynthesis in grown forests. Difficulties with processing data measured in forest canopies usually increase with complexity in canopy architecture, which produces interference in spectral data and enhances the contribution of lower canopy layers to total photosynthesis. Accordingly, the photosynthesis was estimated from representative values of NDVI, PRI and SIFA pointing to phenological as well as physiological processes in the forests. While NDVI changes with amassed vegetation biomass across the season, PRI and fluorescence are considered as indicators of protective mechanisms in plants and photosynthesis. Since both PRI and SIFA show substantial diurnal dynamics associated with canopy NPQ (Acebron et al., 2021), these parameters are considered together.

2.5. Data analysis

Data obtained under conditions of APAR >300 μmol m^{-2} s^{-1} and sun elevations >25° were analyzed to identify seasonal variations of the optical parameters (NDVI, PRI, SIFA, FYSIFA). Data were processed to find a good fit and therefore to identify relationship between modeled and measured canopy photosynthesis data (GPP, LUE) across intervals

of two hours in data measured between 10 and 14 h every day at the highest daily sun elevations. The relationships were examined for only conditions with an average APAR >1200 μmol m^{-2} s^{-1}. The data were evaluated in two hour-long floating windows between 10 and 14 h. The choice of the data (interval) to display was dependent on observed relationships among all variables in the time interval. At Bílý Kříž site we show average data from interval 10:00–12:00, at Štítná site we use data from interval 11:00–13:00.

Each site's dataset was divided into two subsets that were evaluated separately. The GPP dataset covers data acquired in the wider part of the entire growing season. These subsets include the onset of the season with an initial increase in GPP at the forests. The GPP dataset for both stations began on 20th April and ended in mid-September with a daily maximum APAR decrease to below 1200 μmol m^{-2} s^{-1}. The starting date at the Bílý Kříž station was the date of instrument installation. The NDVI dataset was bounded by those dates between which NDVI2 and NDVI1 were constant. Again, we recorded the same starting date for these datasets as 1st June at both sites. The main NDVI datasets for both stations ended in the half of September when the APAR decreased below threshold value. Data from senescing leaves (after September 15th) were not included in the primary analysis. The relationships between parameters in selected subsets at both stations were quantified with coefficients of determination that were evaluated at significance levels $p < 0.05$, < 0.01, and < 0.001. Applicability of Model equations to estimate canopy GPP and LUE was tested also with RMSE.

3. Results

3.1. Dynamic changes in optical parameters

The variations in GPP, LUE, and basic environmental factors at forest sites during the season are shown in Fig. 6. GPP of spruce forest at Bílý

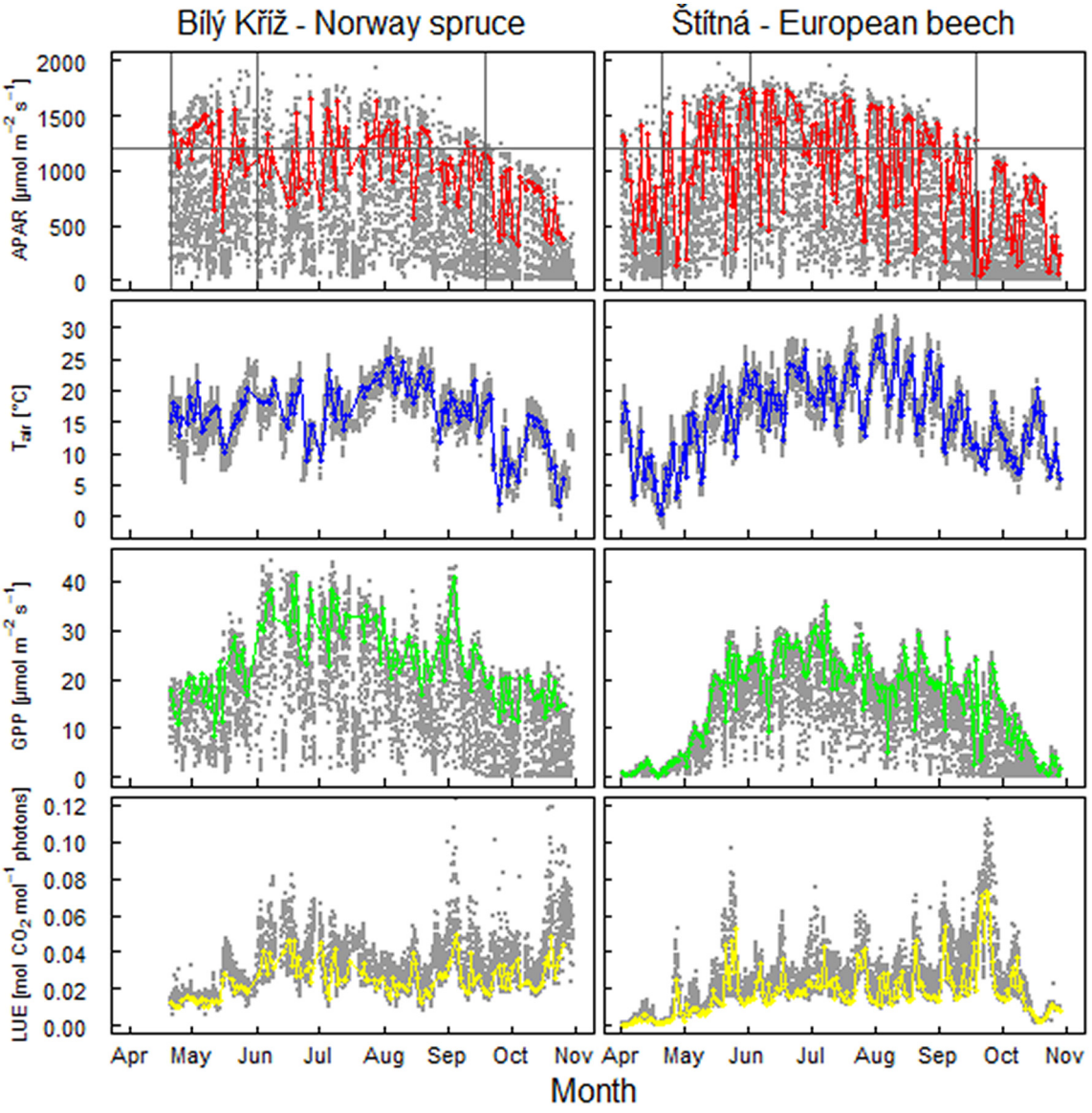

Fig. 6. Changes in the amounts of absorbed photosynthetically active radiation (APAR) by the forests over the season and dynamics of air temperature (T_{air}) at the Bílý Kříž and Štítná ecosystem stations. Average values for measurements at midday are highlighted with colored lines, gray points indicate the variance of the data at half-hourly intervals. Seasonal dynamics of gross primary production (GPP) and light-use efficiency (LUE) of the forests are shown in bottom panels. Gray vertical lines are boundaries in the entire and partial datasets under constant NDVI values.

Kříž station amounted to daily maxima of approximately 20 μmol CO_2 m^{-2} s^{-1} by the end of April when the spectrometer was installed. An increase in GPP in the middle of May was associated with temperature increases. GPP of the beech forest at Štítná station started to rise on 20th April with a gradual increase towards the end of May following the development of leaves. Seasonal dynamics of GPP was characterized by sharp maxima spread across the season reflecting APAR and temperature dynamics. The GPP was decreasing towards autumn; the first pronounced decrease in GPP appeared in August at both sites. Dynamics of photosynthetic LUE followed seasonal light availability (Fig. 6).

Seasonality in foliar development was observed in the dynamics of NDVIs (Fig. 7). PRI dynamics was similar to the dynamics of NDVI2 in spring. The cessation of photosynthesis in beech trees in late autumn returned PRI to its initial state. High PRI values in the evergreen spruce forest throughout the growing season are consistent with NDVI. Daily fluctuations were higher for PRI than for NDVI. We attribute the within-day PRI dynamics to the activity of the xanthophyll cycle with PAR.

SIFA was three-fold higher in the beech than in the spruce forest between June and October (Fig. 8). Coniferous forests have typically lower reflectance of the incoming light as indicated in Fig. 3. SIFA generally increased early in the growing season when leaves developed and photosynthesis functions of the forests were activating. SIFA peaked in both forests soon after the new leaves were developed at the end of May. Fluorescence then gradually decreased following the decrease in APAR and the decrease in GPP. The decrease in SIFA in the spruce forest in the late summer was mirrored by the increase in NDVI2, suggesting SIFA is indeed sensitive to GPP. SIFA detection in the beech forest ended with leaf fall. FYSIFA indicated the onset of the growing season and exhibited a similar trend of decline throughout the season.

3.2. Relationships between optical parameters and GPP and LUE of the forests

Only data from intervals with APAR values exceeding 1200 μmol m^{-2} s^{-1} were used to examine the relationships between reflectance parameters, fluorescence in the O_2A band and stand photosynthesis measures. NDVI2 demonstrated the ability to determine seasonal GPP variations in the deciduous beech forest, with $R^2 = 0.71$ ($p < 0.001$), but also low sensitivity to changes in GPP during the main vegetative period between June and September with $R^2 = 0.29$ (Fig. 9). Our data also confirmed the low potential of NDVI for predicting GPP dynamics in evergreen trees, with a poor regression result ($R^2 = 0.09$; $p < 0.05$). SIFA was significantly correlated ($R^2 = 0.47$; $p < 0.001$) with GPP in the spruce forest (Fig. 9). The relationship between SIFA and GPP, however, was weak in the beech forest showing $R^2 = 0.13$ ($p < 0.01$) for the relationship among the seasonal data.

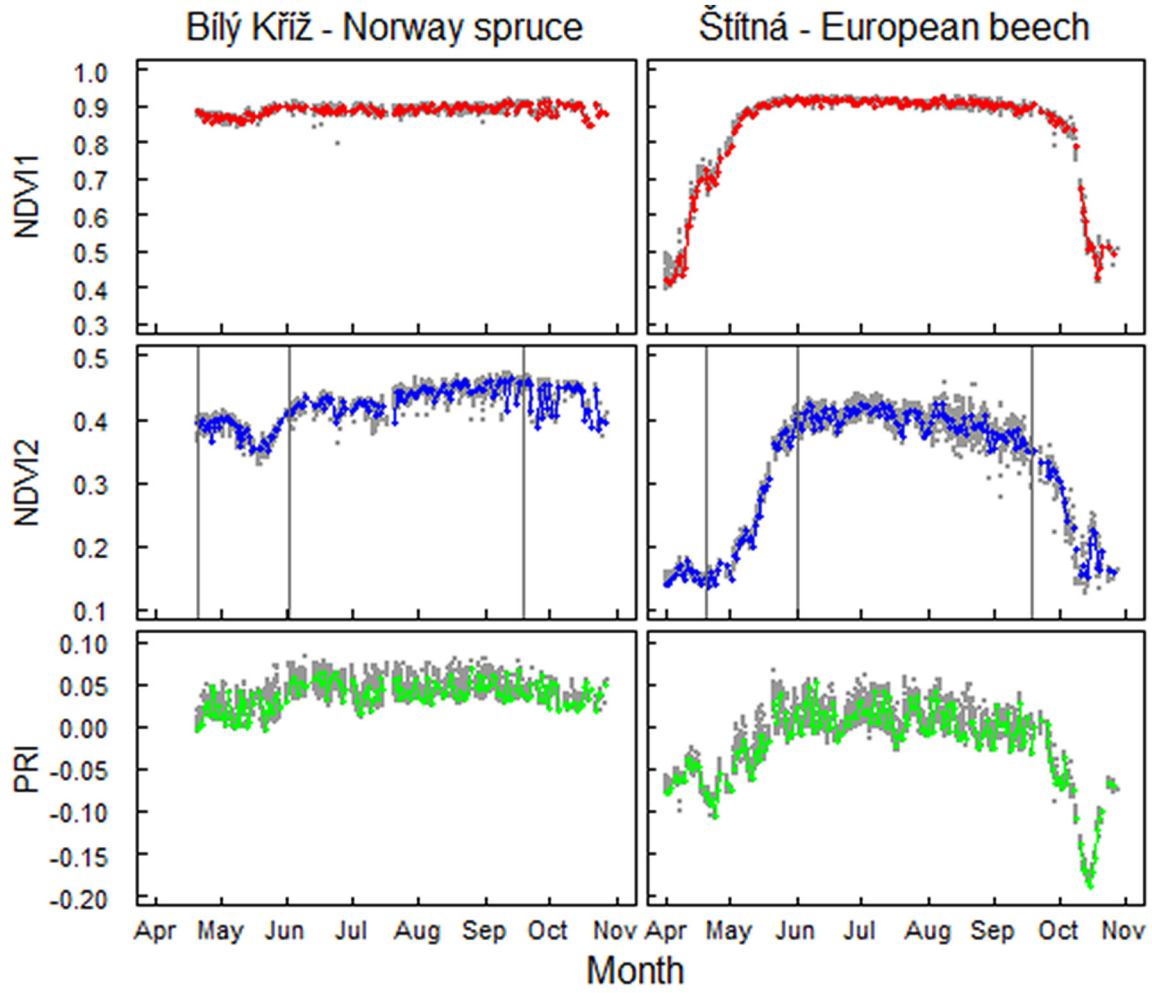

Fig. 7. Seasonal variations in two variants of the normalized difference vegetation index (i.e., NDVI1 and NDVI2) and PRI at the stations with the Norway spruce and European beech trees. The average values for the 2 h long intervals at midday are highlighted with colored points. Gray points highlight the dynamics of the parameters at half-hourly intervals. We show data obtained at APAR >300 μmol m^{-2} s^{-1} and over temporal intervals with tabular sun elevations >25°.

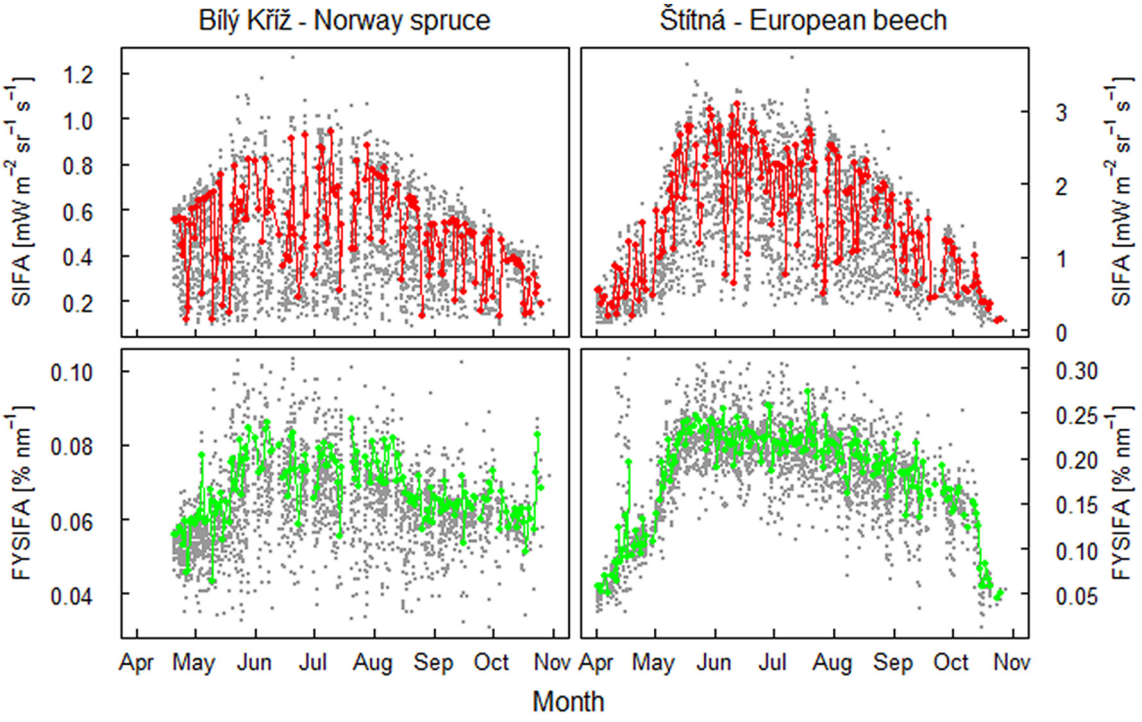

Fig. 8. Dynamic changes in SIFA estimated using the 3-FLD method applied to the radiance data measured for the spruce and beech forests. The yields of these emissions (FYSIFA) are shown in the two bottom panels. Average values for the measurements during the midday 2 h long period are shown with colored points. Gray points indicate the variance of the data in half-hourly intervals during the day, but only those data obtained at APAR >300 μmol m^{-2} s^{-1} and in temporal intervals with sun elevations >25° are shown.

PRI was significantly ($p < 0.001$) correlated with LUE variations over the entire season (Fig. 10) in the beech ($R^2 = 0.66$) and spruce ($R^2 = 0.48$) forests. R^2 values decreased substantially when only the data obtained between June and September were analyzed. FYSIFA in the spruce forest was strongly correlated with LUE ($R^2 = 0.57$; $p < 0.001$) (Fig. 10). Yield of fluorescence was even more strongly correlated with GPP ($R^2 = 0.69$; not shown). However, similar to SIFA–GPP relationship, the connection between FYSIFA and LUE in the beech dataset was low, reaching only $R^2 = 0.19$ ($p < 0.01$) among all data.

The relationship between PRI and LUE was not primarily driven by APAR because PRI and APAR were weakly correlated (Fig. 11), particularly in the beech forest. These results suggest that the observed PRI–LUE dependency is due to adjustments in photosynthetic pigments pools. The result is supported by the close relationship between PRI and NDVI2 (Fig. 12) and stronger correlations between data of the entire season.

According to the data from the spruce forest, the relationship between SIFA and GPP may be driven by the correlation between SIFA and APAR, which is here estimated at $R^2 = 0.46$ ($p < 0.001$, Fig. 10) among all data. The relationship is similar to that observed between SIFA and GPP with $R^2 = 0.47$ ($p < 0.001$). We detected a stronger correlation between SIFA and APAR ($R^2 = 0.69$; $p < 0.001$) in the dataset with constant NDVI, but the correlation between SIFA and GPP ($R^2 = 0.36$; $p < 0.001$) was weaker in this subset. This suggested that the chlorophyll pigments also affected SIFA and estimated dependencies. SIFA variations due to pigments affect positively SIFA–GPP relationships observed across the season. The dependency of SIFA on APAR measured in the beech forest in Fig. 10 was not transferred into SIFA–GPP relationship. Chlorophyll pigments may affect FYSIFA–LUE relationship accordingly, although the estimated connection between NDVI2 and SIFA is not strong (Fig. 12).

The combination of NDVI, PRI, and FYSIFA in the functional models led to substantially higher R^2 values for estimations of canopy LUE. With the use of the Model1 (Eq. (9)) the estimation of canopy LUE in the testing data from the spruce forest was improved and R^2 reached 0.77 ($p < 0.001$, Fig. 13). The RMSE between the predicted and observed LUE values was 0.00285 mol CO_2 per mol of photons. The Model2 (Eq. (10)) for the assessment of LUE in the beech forest showed an R^2 value of 0.63 ($p < 0.001$) in LUE estimation with RMSE equal to 0.00353 mol CO_2 mol^{-1} photons.

In the spruce dataset, the FYSIFA contribution to the estimated value of Model1 (Eq. (9)) decreased towards the end of the season (Fig. 14). That is in accordance with the deactivation of photosynthesis in leaves towards autumn (Fig. 6). We measured a similar but less pronounced trend of a decreasing FYSIFA contribution to the value of the Model2 (Eq. (10)) in data from the beech forest (Fig. 14), but we assume that the observed relationship between Model2 and LUE in the beech forest is weak as a consequence of the weak correlation between FYSIFA and LUE (Fig. 9). FYSIFA contributed to the estimated value of Model parameter in the beech dataset by a higher percentage (>30%) than in the spruce dataset (Fig. 14).

For the spruce dataset, a high contribution of NDVI2 to GPP modeling was detected from the start of measurements in late April (Fig. 14). In contrast, the contribution of NDVI2 to the modeling of GPP in the beech forest gradually increased with foliar development at the start of the season (Fig. 14) and thus provided a basis for efficient GPP modeling. We estimated $R^2 = 0.53$ ($p < 0.001$) with RMSE = 5.95 μmol CO_2 m^{-2} s^{-1} for the GPP estimation from the model equation in the spruce data and $R^2 = 0.58$ ($p < 0.001$) with RMSE = 5.23 μmol CO_2 m^{-2} s^{-1} for the GPP estimation in the beech data (Fig. 13). The R^2 obtained for GPP estimation in beech forest is lower than R^2 estimated in the NDVI2-GPP relationship. On the other hand, the dependencies between the model equations and GPP showed similar slopes for the main vegetative season (June–September) and for the datasets over the entire season. The R^2 are higher among seasonal data.

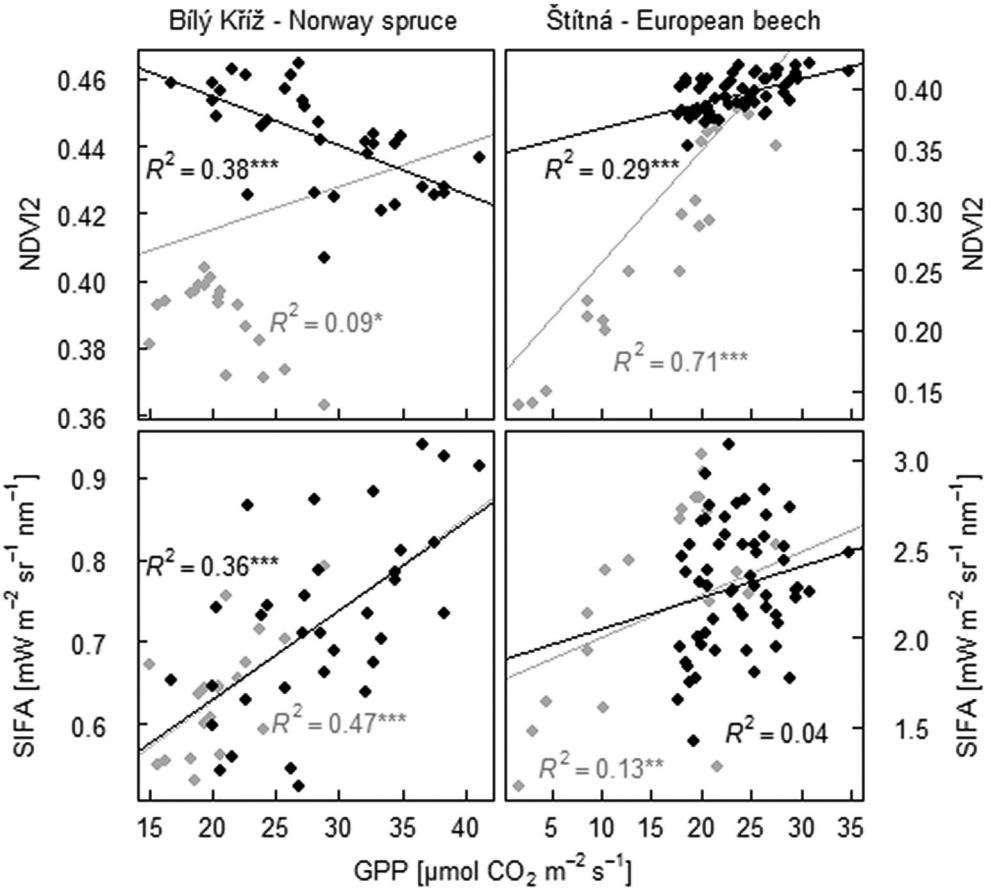

Fig. 9. Relationships of the normalized difference vegetation index (NDVI2) and absolute fluorescence in the O_2A band (SIFA) with gross primary production (GPP) in the spruce and beech forests. Black points represent data obtained between June and September, with almost constant NDVI1 and NDVI2; R^2 values for these relationships are shown with black letters. Gray lines and letters refer to the relationships among all data obtained across the entire season.

4. Discussion

4.1. Relationships of seasonal NDVI and PRI changes with photosynthesis

The ability of remote sensing parameters to track the seasonal course of photosynthesis is often species-specific, since the parameters are sensitive to foliar pigments, which show certain seasonal dynamics dependent on the plant species. Optically measured parameters are often impacted with canopy structure, adding confusion to the data. We present here the seasonal variations in NDVI, PRI, and SIFA – the key optical parameters frequently used to determine photosynthesis dynamics remotely. Data from the hyperspectral system mounted above the forest canopies were integrated over two-hour intervals to reduce impacts of canopy structure on estimated parameters. NDVI, PRI, and SIFA values represent the state of the vegetation at given environmental conditions and in a certain period of the year.

Canopy NDVI was found to be a good indicator of the seasonal GPP trend in deciduous beech forest. This is particularly true for the reflectance at 720 nm, which has a great sensitivity to changes in canopy GPP. Seasonal trend in NDVI of the spruce forest showed low dynamics, because the greenness of coniferous foliage changes only a little across the season. Photosynthetic activity and photoprotective processes in evergreen species involve changes in the organization of the thylakoid membrane and pigment composition throughout the year (Ottander et al., 1995). Seasonal changes in phenology of evergreen species are negligible, but the variations in photosynthesis are substantial as shown in Fig. 5. Such variability is strongly associated with changes in the xanthophyll cycle (Kurasová et al., 2003). Therefore, PRI, which connects remote sensing data to LUE, substantially improves the prediction of photosynthesis in spruce forests. Our dataset from the mountainous spruce forest does not cover the dormancy period before April, in which PRI values are significantly lower in evergreen conifers as indicated by Cheng et al. (2020) and Pierrat et al. (2021).

The correlation between PRI and LUE over the examined period of the year (Fig. 9) may be weakened as a consequence of decoupling during early spring due to different rates of recovery of the chlorophylls:carotenoids ratio and LUE (Fréchette et al., 2015). The effect was apparent in data from both forests in slopes in the PRI-LUE relationships among the two studied subsets. We limit our efforts to exploiting basic relationships under more favorable temperatures that usually follow higher PAR intensities, because PRI may decrease also as a consequence of changes in the physical properties within the leaves with lower temperatures (Kováč et al., 2020; Wong and Gamon, 2015). In given conditions, the relationship between PRI and photosynthesis can be further decoupled by alternative pathways of electron transport in photosystems (Takahashi and Badger, 2011). However, the impact of these processes on PRI sensitivity to LUE in field measurements and particularly for measurements in forests is unclear. The basics of the relationship are likely developed with the seasonality of PRI with variations in pigments as indicated in Gamon et al. (2016).

4.2. Constraints in GPP estimation from SIFA

Changes in SIFA may represent photosynthetic activity because both chlorophyll fluorescence and the xanthophyll cycle are usually involved

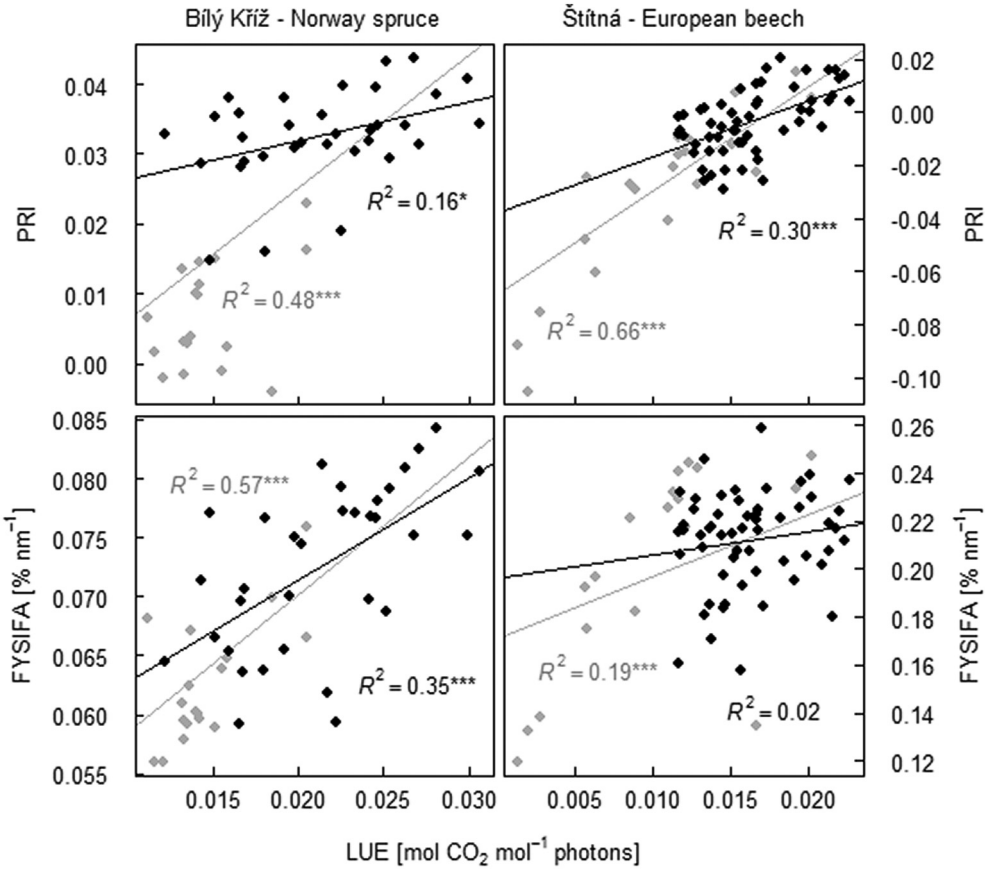

Fig. 10. Relationships of photochemical reflectance index (PRI) and quantum yield of SIFA with light-use efficiency (LUE) in spruce and beech forests. Black lines and adjacent R^2 values refer to relationships in the partial dataset. Gray lines and adjacent R^2 values refer to relationships among all data with average high APAR.

in photoprotection (Cogliati et al., 2015; Pinto et al., 2016). A midday depression in SIFA is typically associated with increased NPQ and low PRI (Paul-Limoges et al., 2018) under conditions of excessive radiation. The link between SIF and photosynthesis depends on the rate of NPQ and is influenced by stress levels because both radiative and nonradiative pathways of dissipation are sensitive to stress conditions (Flexas and Medrano, 2002). Spruce species are especially known to have a high capacity for dynamic NPQ (Kurasová et al., 2003), which is confirmed by the increasing contribution of PRI in the result of the calculated Model1 (Eq. (9)) and decreasing SIF involvement in the modeling of photosynthesis towards the autumn (Fig. 14). Other studies have also found that decreases in SIF due to plant stress, especially under limited water supply, were linked to higher NPQ values (Peguero-Pina et al., 2008). Interval 10–12 h brought better results for estimating photosynthesis in the spruce forest using simple parameters and model equations as compared to other time intervals (not shown). It is similarly difficult to determine if the obstacles in estimation at midday are due to canopy structure or due to physiology, but the result offers suggestion that decreased SIFA is causing impairment in the relationship between SIFA and GPP. Marrs et al. (2020) showed that the observed imbalance between SIFA and GPP is often connected to stomata responses.

The correlation between SIFA and GPP mostly exist due to the dependence of both fluorescence intensity and GPP on incident radiation and on the total exposed foliar area (Joiner et al., 2011; Yang and van der Tol, 2018). Around noon, a large decrease in fluorescence is often associated with photosynthesis decline. In our data, midday FYSIFA of the beech forest remains relatively high during the entire season indicating that also the SIFA is maintained high during the midday hours. Vegetation covers with high midday decline in SIFA have been proclaimed rather as sparse, e.g. crops (Campbell et al., 2019) or younger forests (Paul-Limoges et al., 2018). On the contrary, Yang et al. (2015) showed that SIFA is closely connected to PAR intensity and remains at peak values during midday in old dense forests with a high leaf area index. Therefore, the trend in SIFA and the use of SIFA in GPP estimation can be affected with the maintenance of high SIFA around noon that is related to the age of trees. The measurements at both sites confirmed that the impairments in SIFA-GPP relationships exist due to physiological constraints. The instability in SIFA–GPP relationship was however caused by different factors in each of the forests.

4.3. Selection of fluorescence parameter for modeling photosynthesis

Seasonal dynamics of fluorescence is in accordance with dynamics described by Meroni et al. (2011) or Campbell et al. (2019). Far-red SIF typically increases in spring, peaks in early summer, and then decreases in late summer. Such trend was reported across ecosystems, including grasslands, crops and forests. The changes in SIF primarily reflect changes in chlorophyll amount and PAR intensity as indicated by e.g. Rascher et al. (2015).

Data limited to the period from June to September mostly show weak correlations between physiological measures (GPP, LUE) and optical parameters as presented in Figs. 9, 10 and 13. On the other hand, SIFA–APAR relationship is strong (Fig. 11). The excluded spring period is characterized by the rapid development of plant pigments. Our

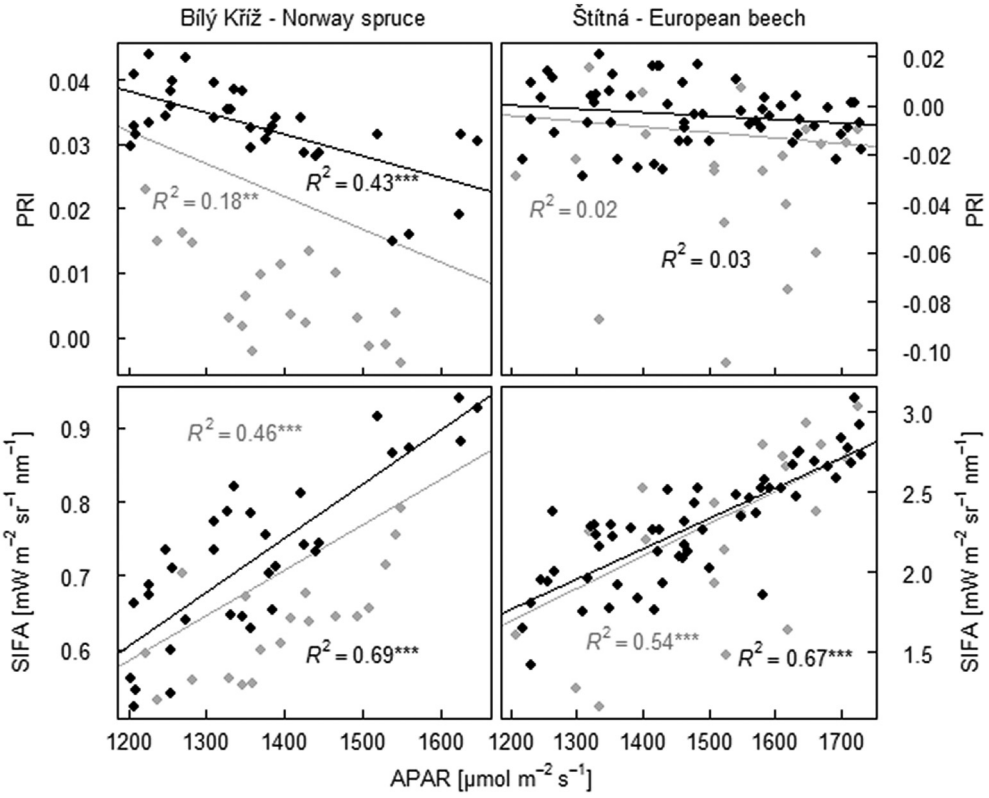

Fig. 11. Dependence of the photochemical reflectance index (PRI) and absolute fluorescence in the O_2A band (SIFA) on APAR. Only data obtained for forest APAR >1200 µmol m^{-2} s^{-1} are evaluated. Gray lines and adjacent R^2 values refer to relationships among seasonal data. Black points and letters refer to data obtained between days with constant NDVIs.

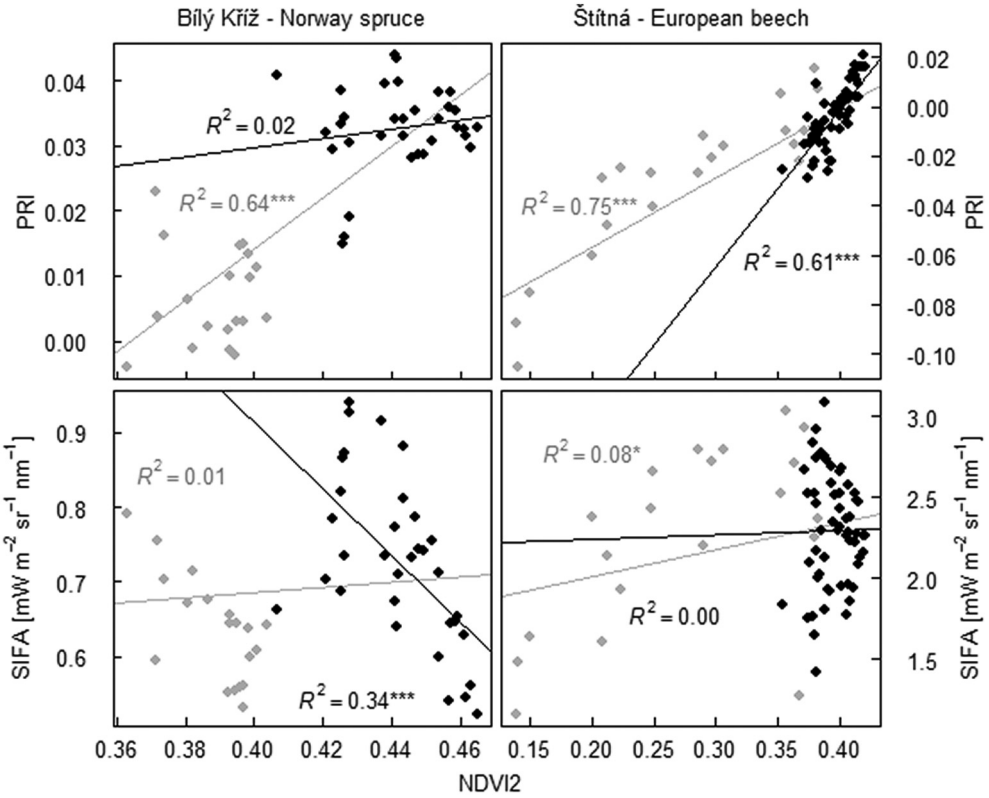

Fig. 12. Relationships of PRI and SIFA with measured NDVI of Norway spruce and European beech forests across entire season (all points) and at peak of the season (black points) datasets. Only the relationships among the data measured in periods with high average APAR of the forests are shown.

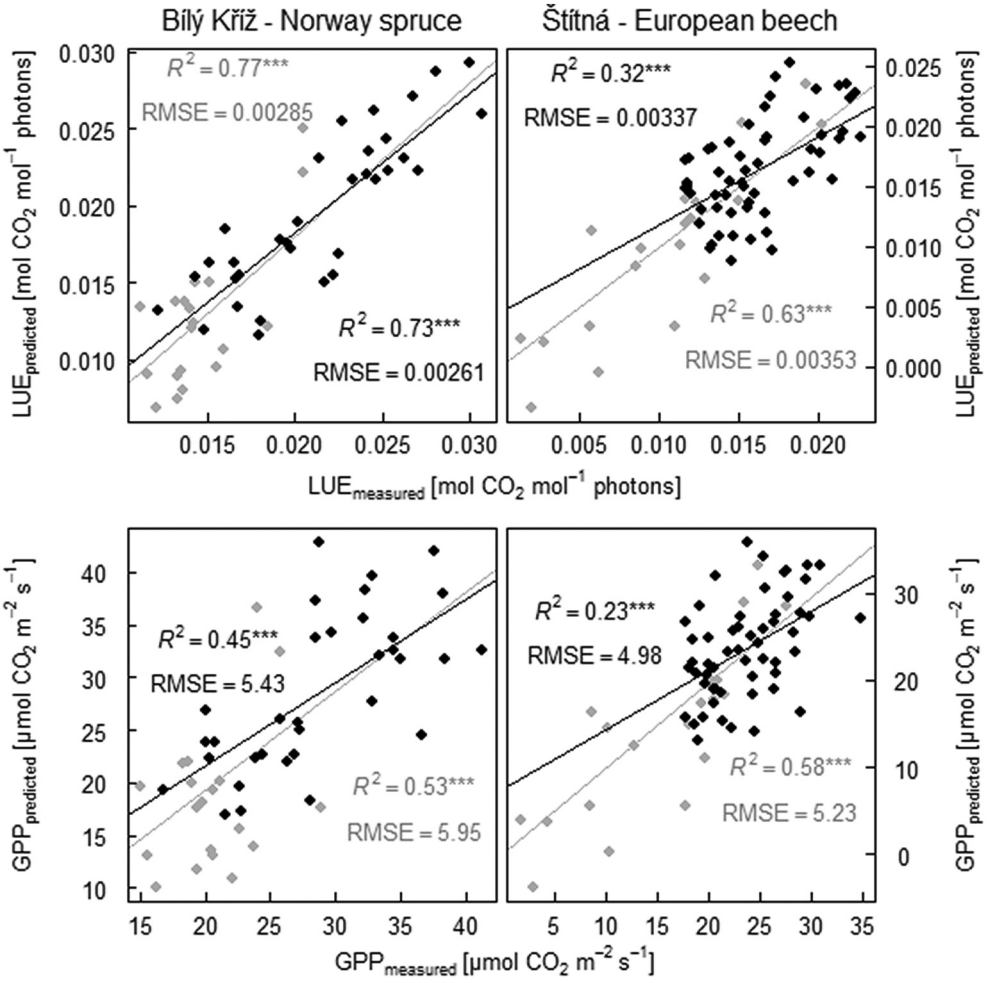

Fig. 13. Accuracy of LUE and GPP estimations from the model equations. Only data obtained at average high APAR levels are evaluated. Gray lines and adjacent R^2 values refer to relationships between all data. Black points and letters refer to data with constant NDVIs.

findings thus support the previous observations by Goulas et al. (2017) and Liu et al. (2017) that the correlation between SIFA and GPP increases with increasing variability in biochemical and structural properties of the studied vegetation. Our dataset indicates that such conclusion is also valid for the correlation between LUE and PRI (Fig. 10).

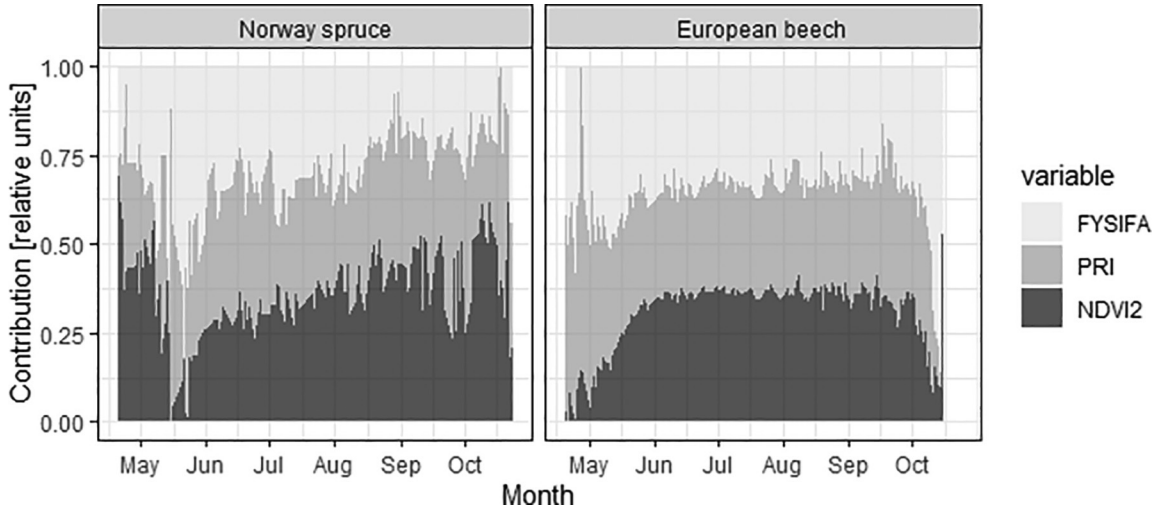

Fig. 14. Contributions of NDVI2, PRI and FYSIFA to the estimated value of the parameter calculated from Model equation in the dataset from Norway spruce forest and in the dataset from European beech forest. Estimates are from the percentage of change in individual parameters throughout the season.

We detected significant and more regular changes in FYSIFA with changes in phenology, mainly with foliar development and senescence accounting for the variations in foliar chlorophyll content (Figs. 8 and 12). This phenomenon has also been reported by Yang et al. (2017), who claimed that biochemical processes in the canopy involve the physiological properties of leaves, especially chlorophyll content. The analysis identified a significant linear correlation between FYSIFA and LUE ($R^2 = 0.56$; $p < 0.001$) in the spruce dataset (Fig. 8). This result is consistent with the previous findings of Yang et al. (2015), Verma et al. (2017), and Miao et al. (2018). SIFA likely contains information regarding both APAR and LUE, i.e., variables determining GPP (GPP = APAR × LUE). As consequence, FYSIFA seems to be an appropriate parameter for photosynthesis modeling and large-scale monitoring of CO_2 uptake by terrestrial ecosystems if we intend to make comparisons with PRI adding a different kind of information.

4.4. Estimation of LUE and GPP from modeling equations

Foliar chlorophyll content and the leaf area index are determinants of ecosystem functionality and therefore inclusion of the parameter describing both variables into the model is necessary to better parametrize carbon fluxes. Correcting the SIFA signal for the effect of canopy structure can help to improve GPP estimations (Nichol et al., 2019). The correction of SIFA for NIR reflectance is considered in numerous studies making estimations of photosynthesis from satellite measurements (Badgley et al., 2017; Yang et al., 2020). The combination of NDVI and PRI has been suggested as a measure of the efficiency with which APAR is converted to fixed carbon (Gamon et al., 2001).

Connection between PRI and FYSIFA offers better links to canopy LUE, since both these variables are modulated by light and show connections to LUE. Verma et al. (2017) achieved a stronger correlation with LUE when SIFA yield was normalized with PRI. Cheng et al. (2013) applied a framework of multiple linear regression to demonstrate the improvement in GPP estimations using red SIF and PRI. Schickling et al. (2016) evaluated an equation that combined NDVI, PRI, and FYSIFA as being very effective for estimating spatial and temporal GPP variations in crop fields, with $R^2 > 0.9$. We used the same principle and similar equations to estimate the variations in photosynthetic efficiency over longer periods in beech and spruce forests. The dependency exists, although the PRI connection to LUE is impacted with many constaints described earlier in the discussion. Estimated parameters showed slightly lower success in determining canopy GPP. The limitation may exist due to fact that we are evaluating multi-layer systems with high canopy leaf area index and we integrate signal only from top canopy layer. We also suggested there are constraints in estimation of photosynthesis from this kind of data due to competitiveness in physiological processes.

It has been shown that spatiotemporal scaling can affect the linearization of the parameters of the flux values (Colombo et al., 2018; van der Tol et al., 2014), so the relationship at a higher scale must be revised. Whether instantaneous space-based information will be comparable to the estimations averaged over two hours that are presented in this study, is not clear. The number of studies comparing NDVI and fluorescence is increasing. The underlying connection between PRI and fluorescence should be further studied, although the studies exist also on this topic (Alonso et al., 2017) and suggest a negative relationship between variables in daily observations and connection of the variables to non-photochemical quenching within the leaves. The studies should also consider PRI variability with pigments and due to canopy structure, which are the factors that often contaminate measured signals in the field and affect relationships to canopy photosynthesis. Data acquisitions from space also presume clear skies, which we did not consider in this study because data from partly cloudy periods were apparently also included in calculations for identifying the relationships. Our analysis, however, indicated that each input to the data product could contribute some information to achieve a better result. Fluorescence signals, together with conventional NDVI and PRI, may be sufficient inputs for models estimating CO_2 fluxes with higher precision.

5. Conclusion

We show seasonal variability of the optical remote sensing signals measured above Norway spruce and European beech forests. The dynamics of NDVI, PRI and SIFA depend on leaf phenological development and actual physiological activity. In particular, we recognized the effects of foliar pigments and NPQ on PRI and SIFA parameters, respectively. Day to day variability in PRI and SIFA parameters were dependent on light availability. While SIFA appeared as an effective indicator of canopy GPP, SIFA yield was in good agreement with canopy LUE. Combining reflectance indices NDVI, PRI, and fluorescence yield in a single equation improved photosynthesis estimation in both deciduous beech and evergreen spruce forests.

CRediT authorship contribution statement

Daniel Kováč: Conceptualization, Supervision, Data curation, Formal analysis, Writing – original draft, Methodology, Visualization. **Alexander Ač:** Methodology. **Ladislav Šigut:** Methodology, Data curation, Visualization. **Josep Peñuelas:** Writing – review & editing. **John Grace:** Writing – review & editing. **Otmar Urban:** Writing – review & editing, Project administration.

Declaration of competing interest

The authors declare that they have no known competing financial interests or personal relationships that could have appeared to influence the work reported in this paper.

Acknowledgements

This work was supported by the Ministry of Education, Youth, and Sports of the Czech Republic within the National Infrastructure for Carbon Observations-CzeCOS (No. LM2015061) and SustES – Adaptation strategies for sustainable ecosystem services and food security under adverse environmental conditions (CZ.02.1.01/0.0/0.0/16_019/0000797). JP also acknowledges funding from the Spanish Government grant PID2019-110521GB-I00, the Catalan government grant SGR2017-1005, and the Fundación Ramón Areces grant ELEMENTAL-CLIMATE.

Appendix A

We recognized that the optical parameters have different sensitivities to forest physiology at different PAR levels. We summarize the relationships in tables, which show coefficients of determination for the relationships between observed variables at different APAR levels. For the measurements in the spruce forest the results are calculated in time window between 10:00–12:00. The results are shown in Appendix A.1. The relationships between variables in the beech forest are calculated in time window between 11:00–13:00, the results are shown in Appendix A.2. It is necessary to address, that selection of different time intervals for evaluation results in involvement of different days into display. Subsets with APAR < 1200 μmol m^{-2} s^{-1} contain also data from autumn. Appendix A.3 shows development of parametric model value over the year.

A.1

Coefficients of determination for the linear relationships between selected parameters measured at the Bílý Kříž ecosystem station with Norway spruce trees. Relationships between the parameters are evaluated at different irradiance levels. Graphs of the measurements at APAR >1200 μmol m^{-2} s^{-1} are shown and discussed in the main text. Average values of the data estimated between 10:00 and 12:00 are shown. N indicates the number of observations in the GPP (NDVI) datasets; *, $p < 0.05$; **, $p < 0.01$; and ***, $p < 0.001$.

Relationship	Dataset	APAR all	APAR >500	APAR >800	APAR >1000	APAR >1200
	N	137 (103)	125 (95)	110 (81)	80 (54)	52 (33)
GPP-NDVI1	GPP	0.12***	0.05*	0.04*	0.09**	0.18**
	NDVI	0.01	0.07**	0.22***	0.44***	0.34***
GPP-NDVI2	GPP	0.08***	0.04*	0.03	0.06*	0.09*
	NDVI	0.00	0.16***	0.29***	0.44***	0.38***
GPP-SIFA	GPP	0.30***	0.16***	0.18***	0.27***	0.48***
	NDVI	0.37***	0.23***	0.23***	0.23***	0.36***
GPP-FYSIFA	GPP	0.40***	0.41***	0.44***	0.49***	0.69***
	NDVI	0.41***	0.35***	0.36***	0.37***	0.55***
LUE-PRI	GPP	0.59***	0.58***	0.55***	0.50***	0.48***
	NDVI	0.52***	0.50***	0.44***	0.35***	0.14*
LUE-FYSIFA	GPP	0.04*	0.12***	0.22***	0.32***	0.56***
	NDVI	0.00	0.02	0.08*	0.11*	0.37***
APAR-PRI	GPP	0.37***	0.37***	0.31***	0.29***	0.18**
	NDVI	0.30***	0.26***	0.20***	0.37***	0.42***
APAR-SIFA	GPP	0.83***	0.80***	0.78***	0.61***	0.46***
	NDVI	0.85***	0.81***	0.81***	0.72***	0.69***
PRI-SIFA	GPP	0.19***	0.14***	0.07**	0.02	0.03
	NDVI	0.21***	0.15***	0.10*	0.23***	0.23*
PRI-NDVI2	GPP	0.10***	0.17***	0.23***	0.41***	0.64***
	NDVI	0.21***	0.17***	0.12*	0.01	0.02
GPP-APAR	GPP	0.14***	0.03	0.02	0.01	0.01
	NDVI	0.26***	0.10**	0.08**	0.06	0.07
LUE-APAR	GPP	0.41***	0.35***	0.24***	0.13**	0.06
	NDVI	0.36***	0.32***	0.20***	0.12*	0.04
LUE- Model1	GPP	0.55***	0.53***	0.60***	0.73***	0.77***
	NDVI	0.55***	0.56***	0.55***	0.58***	0.73***
GPP- Model1	GPP	0.06**	0.19***	0.25***	0.30***	0.53***
	NDVI	0.06*	0.21***	0.29***	0.18***	0.45***

A.2

Coefficients of determination for the linear relationships between selected parameters measured at the Štítná ecosystem station with European beech trees. Relationships between the parameters are evaluated at different irradiance levels. Graphs of the measurements at APAR >1200 μmol m^{-2} s^{-1} are shown and discussed in the main text. The analysis uses average values of the data measured between 11:00 and 13:00; *, $p < 0.05$; **, $p < 0.01$; ***, and $p < 0.001$.

Relationship	Dataset	APAR all	APAR >500	APAR >800	APAR >1000	APAR >1200
	N	170 (94)	141 (85)	117 (74)	105 (70)	76 (56)
GPP-NDVI1	GPP	0.44***	0.55***	0.53***	0.56***	0.53***
	NDVI	0.13***	0.22***	0.27***	0.27***	0.30***
GPP-NDVI2	GPP	0.64***	0.77***	0.79***	0.72***	0.71***
	NDVI	0.05*	0.08**	0.22***	0.21***	0.29***
GPP-SIFA	GPP	0.48***	0.35***	0.29***	0.14***	0.13**
	NDVI	0.38***	0.15***	0.03	0.02	0.04
GPP-FYSIFA	GPP	0.49***	0.46***	0.42***	0.27***	0.29***
	NDVI	0.08**	0.06*	0.05*	0.03	0.08*
LUE-PRI	GPP	0.32***	0.42***	0.52***	0.55***	0.66***
	NDVI	0.55***	0.53***	0.44***	0.44***	0.30***
LUE-FYSIFA	GPP	0.00	0.15***	0.42***	0.12***	0.19***
	NDVI	0.01	0.01	0.00	0.00	0.03
APAR-PRI	GPP	0.01	0.03*	0.04*	0.00	0.02
	NDVI	0.62***	0.48***	0.27***	0.23***	0.03
APAR-SIFA	GPP	0.86***	0.83***	0.76***	0.69***	0.56***
	NDVI	0.87***	0.86***	0.77***	0.71***	0.67***
PRI-SIFA	GPP	0.02	0.17***	0.24***	0.12***	0.11**
	NDVI	0.50***	0.31***	0.10**	0.05	0.01
PRI-NDVI2	GPP	0.59***	0.67***	0.59***	0.66***	0.75***
	NDVI	0.28***	0.48***	0.49***	0.56***	0.61***
GPP-APAR	GPP	0.35***	0.18***	0.10***	0.01	0.00
	NDVI	0.40***	0.13***	0.01	0.00	0.00
LUE-APAR	GPP	0.42***	0.13***	0.04*	0.18***	0.14**
	NDVI	0.77***	0.71***	0.53***	0.46***	0.23***
LUE-Model2	GPP	0.37***	0.48***	0.55***	0.55***	0.63***
	NDVI	0.56***	0.55***	0.45***	0.44***	0.32***

(continued on next page)

(*continued*)

Relationship	Dataset	APAR all	APAR >500	APAR >800	APAR >1000	APAR >1200
	N	170 (94)	141 (85)	117 (74)	105 (70)	76 (56)
GPP-Model2	GPP	0.14***	0.41***	0.49***	0.46***	0.58***
	NDVI	0.14***	0.00	0.10**	0.12**	0.23***

A.3

Seasonal dynamics of gross primary production (GPP) and outputs of the model equations (MODEL eq) applied to spectrometric data from Norway spruce and European beech forests. See Model 1 (spruce) and Model 2 (beech) in the main text. We found that parameter value deteriorates with low temperature. Sudden declines in PRI with temperature, which is apparent also in dynamics shown in Fig. 14 cause apparent breakdowns in the parameter.

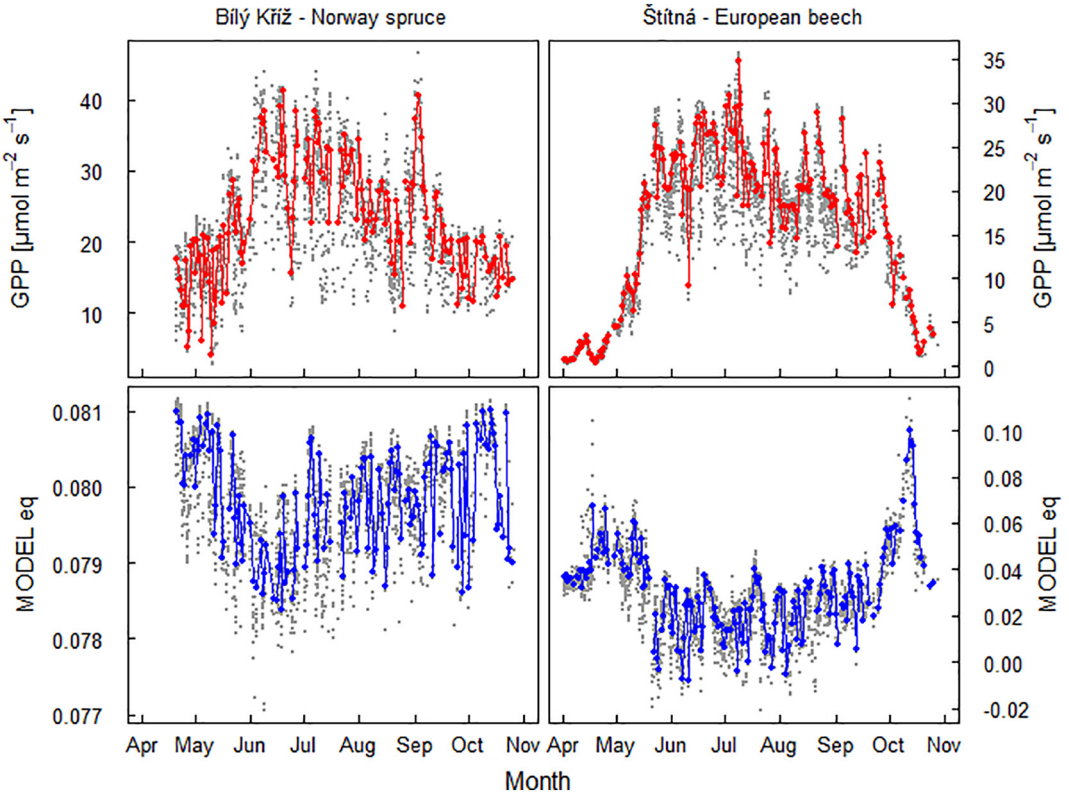

References

Acebron, K., Matsubara, S., Jedmowski, C., Emin, D., Muller, O., Rascher, U., 2021. Diurnal dynamics of nonphotochemical quenching in Arabidopsis npq mutants assessed by solar-induced fluorescence and reflectance measurements in the field. New Phytol. 229, 2104–2119. https://doi.org/10.1111/nph.16984.

Alonso, L., van Wittenberghe, S., Amoros-Lopez, J., Vila-Frances, J., Gomez-Chova, L., Moreno, J., 2017. Diurnal cycle relationships between passive fluorescence, PRI and NPQ of vegetation in a controlled stress experiment. Remote Sens. 9. https://doi.org/10.3390/rs9080770.

Badgley, G., Field, C.B., Berry, J.A., 2017. Canopy near-infrared reflectance and terrestrial photosynthesis. Sci. Adv. 3. https://doi.org/10.1126/sciadv.1602244.

Baldocchi, D.D., 2020. How eddy covariance flux measurements have contributed to our understanding of global change biology. Glob. Chang. Biol. 26, 242–260. https://doi.org/10.1111/gcb.14807.

Barton, C.V.M., North, P.R.J., 2001. Remote sensing of canopy light use efficiency using the photochemical reflectance index model and sensitivity analysis. Remote Sens. Environ. 78, 264–273. https://doi.org/10.1016/S0034-4257(01)00224-3.

Campbell, P.K.E., Huemmrich, K.F., Middleton, E.M., Ward, L.A., Julitta, T., Daughtry, C.S.T., Burkart, A., Russ, A.L., Kustas, W.P., 2019. Diurnal and seasonal variations in chlorophyll fluorescence associated with photosynthesis at leaf and canopy scales. Remote Sens. 11, 488. https://doi.org/10.3390/rs11050488.

Chen, X., Mo, X., Hu, S., Liu, S., 2019. Relationship between fluorescence yield and photochemical yield under water stress and intermediate light conditions. J. Exp. Bot. 70, 301–313. https://doi.org/10.1093/jxb/ery341.

Cheng, Y., Middleton, E.M., Zhang, Q., Huemmrich, K.F., Campbell, P.K.E., Corp, L.A., Cook, B.D., Kustas, W.P., Daughtry, C.S., 2013. Integrating solar induced fluorescence and the photochemical reflectance index for estimating gross primary production in a cornfield. Remote Sens. 5, 6857–6879. https://doi.org/10.3390/rs5126857.

Cheng, R., Magney, T.S., Dutta, D., Bowling, D.R., Logan, B.A., Burns, S.P., Blanken, P.D., Grossmann, K., Lopez, S., Richardson, A.D., Stutz, J., Frankenberg, C., 2020. Decomposing reflectance spectra to track gross primary production in a subalpine evergreen forest. Biogeosciences 17, 4523–4544. https://doi.org/10.5194/bg-17-4523-2020.

Cogliati, S., Rossini, M., Julitta, T., Meroni, M., Schickling, A., Burkart, A., Pinto, F., Rascher, U., Colombo, R., 2015. Continuous and long-term measurements of reflectance and sun-induced chlorophyll fluorescence by using novel automated field spectroscopy systems. Remote Sens. Environ. 164, 270–281. https://doi.org/10.1016/j.rse.2015.03.027.

Colombo, R., Celesti, M., Bianchi, R., Campbell, P.K.E., Cogliati, S., Cook, B.D., Corp, L.A., Damm, A., Domec, J., Guanter, L., Julitta, T., Middleton, E.M., Noormets, A., Panigada, C., Pinto, F., 2018. Variability of sun-induced chlorophyll fluorescence according to stand age-related processes in a managed loblolly pine forest. Glob. Chang. Biol. 24, 2980–2996. https://doi.org/10.1111/gcb.14097.

Damm, A., Elber, J., Erler, A., Gioli, B., Hamdi, K., Hutjes, R., Kosvancova, M., Meroni, M., Miglietta, F., Moersch, A., Moreno, J., Schickling, A., Sonnenschein, R., Udelhoven, T., van der Linden, S., Hostert, P., Rascher, U., 2010. Remote sensing of sun-induced

fluorescence to improve modeling of diurnal courses of gross primary production (GPP). Glob. Chang. Biol. 16, 171–186. https://doi.org/10.1111/j.1365-2486.2009.01908.x.
Datt, B., 1999. A new reflectance index for remote sensing of chlorophyll content in higher plants: tests using Eucalyptus leaves. J. Plant Physiol. 154, 30–36. https://doi.org/10.1016/S0176-1617(99)80314-9.
Daumard, F., Goulas, Y., Champagne, S., Fournier, A., Ounis, A., Olioso, A., Moya, I., 2012. Continuous monitoring of canopy level sun-induced chlorophyll fluorescence during the growth of a sorghum field. IEEE Trans. Geosci. Remote Sens. 50, 4292–4300. https://doi.org/10.1109/TGRS.2012.2193131.
Flexas, J., Medrano, H., 2002. Drought-inhibition of photosynthesis in C-3 plants: stomatal and non-stomatal limitations revisited. Ann. Bot. 89, 183–189. https://doi.org/10.1093/aob/mcf027.
Fréchette, E., Wong, C.Y.S., Junker, L.V., Chang, C.Y.Y., Ensminger, I., 2015. Zeaxanthin-independent energy quenching and alternative electron sinks cause a decoupling of the relationship between the photochemical reflectance index (PRI) and photosynthesis in an evergreen conifer during spring. J. Exp. Bot. 66, 7309–7323. https://doi.org/10.1093/jxb/erv427.
Gamon, J.A., Peñuelas, J., Field, C.B., 1992. A narrow-waveband spectral index that tracks diurnal changes in photosynthetic efficiency. Remote Sens. Environ. https://doi.org/10.1016/0034-4257(92)90059-S.
Gamon, J.A., Field, C.B., Goulden, M.L., Griffin, K.L., Hartley, A.E., Joel, G., Peñuelas, J., Valentini, R., 1995. Relationships between NDVI, canopy structure, and photosynthesis in three Californian vegetation types. Ecol. Appl. 5, 28–41. https://doi.org/10.2307/1942049.
Gamon, J.A., Serrano, L., Surfus, J.S., 1997. The photochemical reflectance index: an optical indicator of photosynthetic radiation use efficiency across species, functional types, and nutrient levels. Oecologia 112, 492–501. https://doi.org/10.1007/s004420050337.
Gamon, J.A., Field, C.B., Fredeen, A.L., Thayer, S., 2001. Assessing photosynthetic downregulation in sunflower stands with an optically-based model. Photosynth. Res. 67, 113–125. https://doi.org/10.1023/A:1010677605091.
Gamon, J.A., Huemmrich, K.F., Wong, C.Y.S., Ensminger, I., Garrity, S., Hollinger, D.Y., Noormets, A., Peñuelas, J., 2016. A remotely sensed pigment index reveals photosynthetic phenology in evergreen conifers. Proc. Natl. Acad. Sci. 113, 13087–13092. https://doi.org/10.1073/pnas.1606162113.
Garbulsky, M.F., Peñuelas, J., Gamon, J., Inoue, Y., Filella, I., 2011. The photochemical reflectance index (PRI) and the remote sensing of leaf, canopy and ecosystem radiation use efficiencies. A review and meta-analysis. Remote Sens. Environ. https://doi.org/10.1016/j.rse.2010.08.023.
Goulas, Y., Fournier, A., Daumard, F., Champagne, S., Ounis, A., Marloie, O., Moya, I., 2017. Gross primary production of a wheat canopy relates stronger to far red than to red solar-induced chlorophyll fluorescence. Remote Sens. 9, 97. https://doi.org/10.3390/rs9010097.
Joiner, J., Yoshida, Y., Vasilkov, A.P., Yoshida, Y., Corp, L.A., Middleton, E.M., Space, G., 2011. First observations of global and seasonal terrestrial chlorophyll fluorescence from space. Biogeosciences 8, 637–651. https://doi.org/10.5194/bg-8-637-2011.
Julitta, T., Corp, L.A., Rossini, M., Burkart, A., Cogliati, S., Davies, N., Hom, M., MacArthur, A., Middleton, E.M., Rascher, U., Schickling, A., Colombo, R., 2016. Comparison of sun-induced chlorophyll fluorescence estimates obtained from four portable field spectroradiometers. Remote Sens. 8. https://doi.org/10.3390/rs8020122.
Kováč, D., Veselovská, P., Klem, K., Večeřová, K., Ač, A., Peñuelas, J., Urban, O., 2018. Potential of photochemical reflectance index for indicating photochemistry and light use efficiency in leaves of European beech and Norway spruce trees. Remote Sens. 10, 1202. https://doi.org/10.3390/rs10081202.
Kováč, D., Veselá, B., Klem, K., Večeřová, K., Materová, Z., Peñuelas, J., Urban, O., 2020. Correction of PRI for carotenoid pigment pools improves photosynthesis estimation across different irradiance and temperature conditions. Remote Sens. Environ. 244, 111834. https://doi.org/10.1016/j.rse.2020.111834.
Kurasová, I., Kalina, J., Urban, O., Štroch, M., Špunda, V., 2003. Acclimation of two distinct plant species, spring barley and Norway spruce, to combined effect of various irradiance and CO_2 concentration during cultivation in controlled environment. Photosynthetica 41, 513–523. https://doi.org/10.1023/B:PHOT.0000027515.05641.fd.
Lasslop, G., Reichstein, M., Papale, D., Richardson, A., Arneth, A., Barr, A., Stoy, P., Wohlfahrt, G., 2010. Separation of net ecosystem exchange into assimilation and respiration using a light response curve approach: critical issues and global evaluation. Glob. Chang. Biol. 16, 187–208. https://doi.org/10.1111/j.1365-2486.2009.02041.x.
Lichtenthaler, H.K., Rinderle, U., 1988. The role of chlorophyll fluorescence in the detection of stress conditions in plants. Crit. Rev. Anal. Chem. 19, S29–S85. https://doi.org/10.1080/15476510.1988.10401466.
Liu, L., Guan, L., Liu, X., 2017. Directly estimating diurnal changes in GPP for C3 and C4 crops using far-red sun-induced chlorophyll fluorescence. Agric. For. Meteorol. 232, 1–9. https://doi.org/10.1016/j.agrformet.2016.06.014.
Marrs, J.K., Reblin, J.S., Logan, B.A., Allen, D.W., Reinmann, A.B., Bombard, D.M., Tabachnik, D., Hutyra, L.R., 2020. Solar-induced fluorescence does not track photosynthetic carbon assimilation following induced stomatal closure. Geophys. Res. Lett. 47. https://doi.org/10.1029/2020GL087956.
McGloin, R., Šigut, L., Pavelka, M., Sedlák, P., 2018. Energy balance closure at a variety of ecosystems in Central Europe with contrasting topographies. Agric. For. Meteorol. 248, 418–431. https://doi.org/10.1016/j.agrformet.2017.10.003.
Meroni, M., Rossini, M., Guanter, L., Alonso, L., Rascher, U., Colombo, R., Moreno, J., 2009. Remote sensing of solar-induced chlorophyll fluorescence: review of methods and applications. Remote Sens. Environ. 113, 2037–2051. https://doi.org/10.1016/j.rse.2009.05.003.
Meroni, M., Barducci, A., Cogliati, S., Castagnoli, F., Rossini, M., Busetto, L., Migliavacca, M., Cremonese, E., Galvagno, M., Colombo, R., DiCella, U.M., 2011. The hyperspectral irradiometer, a new instrument for long-term and unattended field spectroscopy measurements. Rev. Sci. Instrum. 82, 43106. https://doi.org/10.1063/1.3574360.
Miao, G., Guan, K., Yang, X., Bernacchi, C.J., Berry, J.A., DeLudia, E.H., 2018. Sun-induced chlorophyll fluorescence, photosynthesis, and light use efficiency of a soybean field from seasonally continuous measurements. J. Geophys. Res. Biogeosci. 123, 610–623. https://doi.org/10.1002/2017JG004180.
Nichol, C.J., Huemmrich, K.F., Black, T.A., Jarvis, P.G., Walthall, C.L., Grace, J., Hall, F.G., 2000. Remote sensing of photosynthetic-light-use efficiency of boreal forest. Agric. For. Meteorol. 101, 131–142. https://doi.org/10.1016/S0168-1923(99)00167-7.
Nichol, C.J., Drolet, G., Porcar-Castell, A., Wade, T., Sabater, N., Middleton, E.M., Maclellan, C., Levula, J., Mammarella, I., Vesala, T., Atherton, J., 2019. Diurnal and seasonal solar induced chlorophyll fluorescence and photosynthesis in a boreal scots pine canopy. Remote Sens. 11, 273. https://doi.org/10.3390/rs11030273.
Ottander, C., Campbell, D.A., Oquist, G., 1995. Seasonal changes in photosystem II organization and pigment composition in pinus silvestris. Planta 197, 176–183. https://doi.org/10.1007/BF00239954.
Pacheco-Labrador, J., Martin, M.P., 2014. Nonlinear response in a field portable spectroradiometer: characterization and effects on output reflectance. IEEE Trans. Geosci. Remote Sens. 52, 920–928. https://doi.org/10.1109/TGRS.2013.2245671.
Pan, Y., Birdsey, R.A., Fang, J., Houghton, R., Kauppi, P.E., Kurz, W.A., Phillips, O.L., Shvidenko, A., Lewis, S.L., Canadell, J.G., Ciais, P., Jackson, R.B., Pacala, S.W., McGuire, A.D., Piao, S., Rautiainen, A., Sitch, S., Hayes, D., 2011. A large and persistent carbon sink in the world's forests. Science 333, 988–993. https://doi.org/10.1126/science.1201609.
Papale, D., Reichstein, M., Aubinet, M., Canfora, E., Bernhofer, C., Kutsch, W., Longdoz, B., Rambal, S., 2006. Towards a standardized processing of net ecosystem exchange measured with eddy covariance technique: algorithms and uncertainty estimation. Biogeosciences 3, 571–583. https://doi.org/10.5194/bg-3-571-2006.
Paul-Limoges, E., Damm, A., Hueni, A., Liebisch, F., Eugster, W., Schaepman, M.E., Buchmann, N., 2018. Effect of environmental conditions on sun-induced fluorescence in a mixed forest and a cropland. Remote Sens. Environ. 219, 310–323. https://doi.org/10.1016/j.rse.2018.10.018.
Peguero-Pina, J.J., Morales, F., Flexas, J., Gil-Pelegrín, E., Moya, I., 2008. Photochemistry, remotely sensed physiological reflectance index and de-epoxidation state of the xanthophyll cycle in Quercus coccifera under intense drought. Oecologia 156, 1–11. https://doi.org/10.1007/s00442-007-0957-y.
Peñuelas, J., Filella, I., Gamon, J.A., 1995. Assessment of photosynthetic radiation-use efficiency with spectral reflectance. New Phytol. 131, 291–296. https://doi.org/10.1111/j.1469-8137.1995.tb03064.x.
Peñuelas, J., Garbulsky, M.F., Filella, I., 2011. Photochemical reflectance index (PRI) and remote sensing of plant CO_2 uptake. New Phytol. https://doi.org/10.1111/j.1469-8137.2011.03791.x.
Perez-Priego, O., Zarco-Tejada, P.J., Miller, J.R., Sepulcre-Cantó, G., Fereres, E., 2005. Detection of water stress in orchard trees with a high-resolution spectrometer through chlorophyll fluorescence in-filling of the O_2A band. IEEE Trans. Geosci. Remote Sens. 43, 2860–2869. https://doi.org/10.1109/TGRS.2005.857906.
Pierrat, Z., Nehemy, M.F., Roy, A., Magney, T., Parazoo, N.C., Laroque, C., Pappas, C., Sonnentag, O., Grossmann, K., Bowling, D.R., Seibt, U., Ramirez, A., Johnson, B., Helgason, W., Barr, A., Stutz, J., 2021. Tower-based remote sensing reveals mechanisms behind a two-phased spring transition in a mixed-species boreal forest. J. Geophys. Res. 126. https://doi.org/10.1029/2020JG006191.
Pinto, F., Damm, A., Schickling, A., Panigada, C., Cogliati, S., Müller-Linow, M., Balvora, A., 2016. Sun-induced chlorophyll fluorescence from high-resolution imaging spectroscopy data to quantify spatio-temporal patterns of photosynthetic function in crop canopies. Plant Cell Environ. 39, 1500–1512. https://doi.org/10.1111/pce.12710.
Plascyk, J.A., 1975. The MK II Fraunhofer line discriminator (FLD-II) for airborne and orbital remote sensing of solar-stimulated luminescence. Opt. Eng. 14, 339–346. https://doi.org/10.1117/12.7971842.
R Core Team, 2020. R: A Language and Environment for Statistical Computing. R Foundation for Statistical Computing, Vienna, Austria. https://www.R-project.org/.
Rascher, U., Alonso, L., Burkart, A., Cilia, C., Cogliati, S., Colombo, R., 2015. Sun-induced fluorescence – a new probe of photosynthesis: first maps from the imaging spectrometer HyPlant. Glob. Chang. Biol. 21, 4673–4684. https://doi.org/10.1111/gcb.13017.
Reichstein, M., Falge, E., Baldocchi, D.D., Papale, D., Aubiet, M., Berbigier, P., Bernhofer, C., Buchmann, N., Gilmanov, T., Granier, A., Grunwald, T., Havránková, K., Ilvesniemi, H., Janouš, D., Knohl, A., Luurila, T., Lohila, A., Loustau, D., Matteucci, G., Meyers, T., Miglietta, F., Ourcival, J.-M., Pumpanen, J., Rambal, S., Rotenberg, E., Sanz, M., Tenhunen, J., Seufert, G., Vaccari, F., Vesala, T., Yakir, D., Valentini, R., 2005. On the separation of net ecosystem exchange into assimilation and ecosystem respiration: review and improved algorithm. Glob. Chang. Biol. 11, 1424–1439. https://doi.org/10.1111/j.1365-2486.2005.001002.x.
Schickling, A., Matveeva, M., Damm, A., Schween, J.H., Wahner, A., Graf, A., Crewell, S., Rascher, U., 2016. Combining sun-induced chlorophyll fluorescence and photochemical reflectance index improves diurnal modeling of gross primary productivity. Remote Sens. 8, 574. https://doi.org/10.3390/rs8070574.
Takahashi, S., Badger, M.R., 2011. Photoprotection in plants: a new light on photosystem II damage. Trends Plant Sci. 16, 53–60. https://doi.org/10.1016/j.tplants.2010.10.001.
van der Tol, C., Berry, J.A., Campbell, P.K.E., Rascher, U., 2014. Models of fluorescence and photosynthesis for interpreting measurements of solar-induced chlorophyll fluorescence. J. Geophys. Res. Biogeosci. 119, 2312–2327. https://doi.org/10.1002/2014JG002713.We.
Verma, M., Schimel, D., Evans, B., Frankenberg, C., Beringer, J., Eldering, A., 2017. Effect of environmental conditions on the relationship between solar-induced fluorescence and gross primary productivity at an OzFlux grassland site. J. Geophys. Res. Biogeosci. 2, 716–733. https://doi.org/10.1002/2016JG003580.
Wieneke, S., Burkart, A., Cendrero-Mateo, M.P., Julitta, T., Rossini, M., Schickling, A., 2018. Linking photosynthesis and sun-induced fluorescence at sub-daily to seasonal scales. Remote Sens. Environ. 219, 247–258. https://doi.org/10.1016/j.rse.2018.10.019.

van Wittenberghe, S., Alonso, L., Verrelst, J., Hermans, I., Delegido, J., Veroustraete, F., Valcke, R., Moreno, J., Samson, R., 2013. Upward and downward solar-induced chlorophyll fluorescence yield indices of four tree species as indicators of traffic pollution in Valencia. Environ. Pollut. 173, 29–37. https://doi.org/10.1016/j.envpol.2012.10.003.

Wong, C.Y.S., Gamon, J.A., 2015. Three causes of variation in the photochemical reflectance index (PRI) in evergreen conifers. New Phytol. 206, 187–195. https://doi.org/10.1111/nph.13159.

Wutzler, T., Lucas-Moffat, A., Migliavacca, M., Knauer, J., Sickel, K., Šigut, L., 2018. Basic and extensible post-processing of eddy covariance flux data with REddyProc. Biogeosciences 15, 5015–5030. https://doi.org/10.5194/bg-15-5015-2018.

Yang, P., van der Tol, C., 2018. Linking canopy scattering of far-red sun-induced chlorophyll fluorescence with reflectance. Remote Sens. Environ. 209, 456–467. https://doi.org/10.1016/j.rse.2018.02.029.

Yang, X., Tang, J., Mustard, J.F., Lee, J., Rossini, M., Joiner, J., Munger, J.W., Kornfeld, A., Richardson, A.D., 2015. Solar-induced chlorophyll fluorescence that correlates with canopy photosynthesis on diurnal and seasonal scales in a temperate deciduous forest. Geophys. Res. Lett. 42, 2977–2987. https://doi.org/10.1002/2015GL063201.Received.

Yang, P., Verhoef, W., van der Tol, C., 2017. The mSCOPE model: a simple adaptation to the SCOPE model to describe reflectance, fluorescence and photosynthesis of vertically heterogeneous canopies. Remote Sens. Environ. 201, 1–11. https://doi.org/10.1016/j.rse.2017.08.029.

Yang, P., van der Tol, C., Campbell, P.K.E., Middleton, E.M., 2020. Fluorescence correction vegetation index (FCVI): a physically based reflectance index to separate physiological and non-physiological information in far-red sun-induced chlorophyll fluorescence. Remote Sens. Environ. 240, 111676. https://doi.org/10.1016/j.rse.2020.111676.

Zarco-Tejada, P.J., Miller, J.R., Mohammed, G.H., Noland, T.L., 2000. Chlorophyll fluorescence effects on vegetation apparent reflectance: I. Leaf-level measurements and model simulation. Remote Sens. Environ. 74, 582–595. https://doi.org/10.1016/S0034-4257(00)00148-6.

Zhang, C., Filella, I., Garbulsky, M.F., Peñuelas, J., 2016. Affecting factors and recent improvements of the Photochemical Reflectance Index (PRI) for remotely sensing foliar, canopy and ecosystemic radiation-use efficiencies. Remote Sens. 8. https://doi.org/10.3390/rs8090677.

Zhang, Z., Zhang, Y., Zhang, Q., Chen, J.M., Porcar-Castell, A., Guanter, L., Wu, Y., Zhang, X., Wang, H., Ding, D., Li, Z., 2020. Assessing bi-directional effects on the diurnal cycle of measured solar-induced chlorophyll fluorescence in crop canopies. Agric. For. Meteorol. 295. https://doi.org/10.1016/j.agrformet.2020.108147.